Journal of Analytical Science and Technology

RESEARCH ARTICLE Open Access

Assessment of the antibacterial efficacy of silver nanoparticles-based *Artemisia annua* against methicillin-resistant *Staphylococcus aureus*-infected lung tissues in albino rats

Mohamed T. Shaaban[1], Marwa Salah Abdel-Hamid[2*], Sahar H. Orabi[3], Reda M. S. Korany[4] and Rania Hamed Elbawab[1]

Abstract

The production of alternative and effective medicines is crucial given that antibiotic resistance is currently a global health concern. Several biochemical identification tests were used to screen for *Staphylococcus aureus* isolates. Analysis of *Artemisia annua* extract was performed using a trace GC–mass spectrometer, which revealed that the *A. annua* extract contains numerous compounds, such as artemisinins, palmitic acid and other vital essential compounds that have antioxidant and anti-inflammatory properties. The isolate st.8 was resistant to cefoxitin, oxacillin, and cephalosporins; furthermore, MALDI-TOF/MS Biotyper® identified it as methicillin-resistant *S. aureus* with confidence value 99.9% of mass spectrum compared with reference spectra. The synthesis of green silver nanoparticles based on *A. annua* as a reducing agent was confirmed via partial characterizations: (HR-TEM), (XRD), (SEM), (EDX) and (FTIR) analysis. The significant of antibacterial activity of the new green material (AgNPs) was achieved by determining the agar well diffusion assay. Furthermore, compared with those in the Staphylococcus-infected group, a significant decrease in hematological parameters was observed, with an increase in antioxidant biomarkers, a decrease in interstitial tissue thickening by inflammatory cells, and a weak positive immune reaction in a few cells (TNF-α and iNOS) in rats. Overall, this study is a promising step toward the development of new and effective strategies for combating MRSA infections.

Keywords Methicillin-resistant *Staphylococcus aureus*, *Artemisia annua*, Green silver nanoparticles, Lung infection, Antibacterial efficacy

Introduction

Staphylococcus aureus infections can take many different forms and pose a major threat to all human life. Methicillin-resistant *S. aureus* is one of the most prevalent nosocomial infections; it exhibits a multidrug resistance (MDR) phenotype and is not susceptible to β-lactam antibiotics (Baede et al. 2022). The high pathogenicity of *S. aureus* causes recurrent nosocomial and community-related infections, so continuous isolation and identification of these strains are highly important for timely treatment. In addition, virulence genes play an important role in the pathogenicity of *S. aureus* strains (Loges et al. 2020). *S. aureus* employs different virulence agents,

*Correspondence:
Marwa Salah Abdel-Hamid
marwa.salah@gebri.usc.edu.eg
[1] Botany and Microbiology Department, Faculty of Science, Menoufia University, Shibin El Kom, Egypt
[2] Microbial Biotechnology Department, Genetic Engineering and Biotechnology Research Institute, University of Sadat city, Menoufia governorate, Sadat city, Egypt
[3] Biochemistry and Chemistry of Nutrition Department, Faculty of Veterinary Medicine, University of Sadat city, Menoufia governorate, Sadat city, Egypt
[4] Pathology Department, Faculty of Veterinary Medicine, Cairo University, Giza, Egypt

including enzymes, toxins, adhesion proteins, and cell surface proteins that attach to tissue and contribute to the formation of biofilms. Many toxins and enzymes are involved in the spread and colonization of bacteria, tissue damage, cytolytic activity, and proinflammatory activity (Arciola et al. 2018). Additionally, the lysis of host cells by *S. aureus* leads to infection. *S. aureus* can result in serious skin and soft tissue infections, endocarditis, septic arthritis, pneumonia, osteomyelitis, and otitis media (Turner et al. 2019). Several virulence factors are used by *S. aureus* strains to infect the host and create resistance (Liu et al. 2021). The overuse and prolonged use of antibiotics have led to an international issue known as antibiotic-resistant bacteria (Baptista et al. 2018). Therefore, the use of nanotechnology is an innovative treatment for MDR bacteria. Owing to their physical and biological characteristics (particles between 1 and 100 nm in size), nanoparticles can offer solutions for incurable diseases through technical issues such as environmental contamination and medication (Bahrulolum et al. 2021). AgNPs have strong antibacterial potential against both gram-positive and gram-negative bacteria (Srikar et al. 2016). AgNPs can be made using a variety of approaches, including chemical, electrochemical, radiation, and photochemical approaches. However, the physical and chemical synthesis of AgNPs might result in high costs, low efficiency, environmental pollution, and hazardous impacts on human health (Castillo-Henríquez et al. 2020). Biological techniques known as "green synthesis" consider safe, nontoxic substances and involve the use of plant, bacterial, and algal extracts as reducing and capping agents (Aromal and Philip 2012). AgNPs have diverse applications in medicine, including their use as medicines, antioxidants, antibacterial agents, and cytotoxic agents (Baptista et al. 2018; Shelembe et al. 2022; Zhang et al. 2023).

Traditional medicinal plants and herbal compounds have been extensively used worldwide for the treatment of various diseases (Bisht et al. 2021). The Artemisia genus, which belongs to the Asteraceae family, comprises approximately 250 species, some of which contain secondary metabolites such as acids, flavonoids, alkaloids, and terpenoids and play crucial roles in the green synthesis of metal nanoparticles (Carvalho et al. 2011). Artemisia species, including *A. annua*, are commonly used to treat malaria, hepatitis, cancer, fever, inflammation, and wound healing and exhibit antibacterial, antifungal, and disinfecting properties (Adoni et al. 2020).

A. annua extracts contain various chemical compounds, including essential oils, terpenoids, and flavonoids, which facilitate the reduction, capping, and stabilization of Ag ions during biosynthesis; these extracts were analyzed using various spectroscopic techniques, and their antibacterial activity, free radical scavenging ability, color degradation potential, and impact on seed germination were evaluated (Appalasamy et al. 2014).

Artemisinins derived from *A. annua* have shown concentration-dependent and specific antimicrobial effects against gram-positive and gram-negative bacteria, as well as fungi (Goswami et al. 2012). They exhibit direct or synergistic antimicrobial actions against clinically resistant and pathogenic microorganisms, including *Helicobacter pylori*, *Staphylococcus aureus*, *Mycobacterium tuberculosis*, and the hepatitis C virus. Furthermore, condensate tannins from *A. annua* extracts demonstrate significant anti-HSV-2 activity and may cause resistance against HBV, while artemisinins have inhibitory effects on the hepatitis C virus JFH-1 (Tao et al. 2020). However, further research is needed to enhance the clinical use of artemisinins. This study aimed to isolate of new Egyptian clinical MRSA *Staphylococcus aureus*, which was selected and identified using MALDI-TOF/MS Biotyper. In addition, synthesize green silver nanoparticles based on *Artemisia annua* extract, and study their physiochemical characteristics. Moreover, evaluate the protective effects of *A. annua*-AgNPs against *S. aureus*-induced lung pneumonia in rats and assess their antioxidant and anti-inflammatory effects.

Materials and methods

Chemicals

The experiment employed high-quality chemicals throughout. Silver nitrate ($AgNO_3$) was sourced from Merck (Germany), while all bacterial growth media components and ethanol solution obtained from Sigma-Aldrich™. *A. annua* leaves were purchased from the Harraz market for the food industry and natural products in Egypt. Distilled water served for the experiments, while deionized Millipore water was used in nanoparticles preparations.

Clinical samples collection

The bacterial isolates were obtained from patients in the intensive care unit (ICU) of the main hospital of Menoufyia University in Egypt. A total of 30 clinical samples were collected from 30 patients, including 11 males and 19 females, ranging in age from 21 to 70 years. A total of 9 sputum samples, 4 pus wound samples, and 17 blood samples were used for the screening and isolation of *S. aureus* isolates. The specimens were collected following the guidelines of the European Committee on Antimicrobial Susceptibility Testing (EUCAST).

Screening of *Staphylococcus aureus* isolates

The samples were streaked on blood agar and incubated aerobically at 37°C for 24 h. The screening of *S. aureus* isolates was based on colony morphology and gram staining. Further confirmation of the suspected *S. aureus* isolates was performed through the growth of yellow colonies on mannitol salt agar (Obeid et al. 2013), the tube coagulase test (Asif et al. 2021), the DNase test (Holt et al. 1994), and the catalase test (Rushdy et al. 2007). Two bacterial reference strains, *S. aureus* ATCC 25923 and *Escherichia coli*, kindly provided positive control strains for the tests from the Microbial Biotechnology Department of the Genetic Engineering and Biotechnology Research Institute at the University of Sadat City, Menoufyia Governorate, Egypt.

Preparation of *Artemisia annua* extract

The leaves were cleaned and dried in an oven at 50°C for three days. Subsequently, the plants were pulverized using a sterile mortar (Moulinex). Twenty-five grams of *A. annua* powder was then extracted with 100 ml of 70% and 96% ethanol alcohol with intermittent shaking at room temperature for 48 h (Recio et al. 1989). The obtained extracts were filtered using Whatman No. 4 filter paper (Grade 4 V; Sigma-Aldrich). The filtrate was stored at 4°C until its inhibitory effect was assessed.

Gas chromatography (GC–MS) analysis of *Artemisia annua*

The *A. annua* ethanolic extract was analyzed using GC–MS. A trace GC-ISQ mass spectrometer with a TG–5MS column was used. The temperature was varied from 50°C to 200°C at 5°C/min and then to 300°C at 25°C/min. Injector and MS transfer line: 270°C and 260°C. Helium carrier gas. Solvent delay: 4 min. An AutoSampler AS1300 was used to inject 1 µl of diluted sample. EI mass spectra collected in the m/z 50–650 range. The component ID was determined by comparing the retention times and spectra with those of the WILEY 09 and NIST 14 databases (Abd El-Kareem et al. 2016).

Synthesis of silver nanoparticles using *Artemisia annua* extract as a reducing agent

A 1 mM silver nitrate solution was prepared by dissolving 0.017 g of AgNO3 in 100 ml of double distilled water. The plant extract and silver nitrate were mixed at a 1:9 ratio (v/v). The mixture was heated and stirred at 60–80°C and 300 rpm using a magnetic stirrer. Within 10 min to 1 h, the mixture turned reddish brown, indicating nanoparticle formation. Green nanoparticles were separated by centrifugation at 15,000 rpm for 45 min. The precipitated nanoparticles were lyophilized and stored in a cool, dry, and dark place for further physiochemical characterization (Ashraf et al. 2016).

Partial characterizations of the green silver nanoparticles synthesized from *Artemisia annua*

UV–visible spectroscopy

The creation of AgNPs and the optical properties of the nanoparticles were assessed by measuring the absorbance in the range of 200–800 nm using a T80þUV-Vis spectrometer.

HR-transmission electron microscopy (TEM)

The size, shape, and assembly of the nanoparticles were estimated using a JEM-2100 TEM instrument. The nanoparticle suspension was sonicated for 10 min using a Crest Ultrasonics Corp. instrument. A few drops of the suspension were loaded onto a carbon-coated copper grid and left to dry. The dried samples were then observed using TEM.

Scanning electron microscopy (SEM)

The size, surface morphology, and scattering of the nanoparticles were measured using a JEOL JSM-6100 SEM instrument equipped with an EDX sensor system. The instrument was operated at a practical potential of 20 kV and was adjusted before the images were recorded.

X-ray diffraction (XRD)

Crystal phase identification of the nanoparticles was performed using a powder XRD instrument. Two different XRD instruments, PW 3040/60 Philips X'Pert (Holland) and PAN analytical X-Pert PRO, were used. Cu (Kα) radiation was applied at a wavelength (ʎ) of 0.15416 nm. XRD analysis provided information about the crystalline phases present in the nanoparticles (Vijayalakshmi and Rajendran 2012).

Fourier transform infrared (FTIR)

The identification of functional groups and biomolecules responsible for the reduction of silver ions and capping of the silver nanoparticles was conducted using a spectrometer (FTIR-6100 type A). The spectra were recorded in the wavelength range of 400 to 4000 cm^{-1}. This analysis provided information about the specific chemical bonds and biomolecules involved in the synthesis and stabilization of silver nanoparticles (Kim et al. 2017).

In vitro antibacterial assay of the new green silver nanoparticles

The antibacterial activity of the ethanolic extracts was evaluated using the agar well diffusion method (Perez et al. 1990) following the guidelines of the National Committee for Clinical Laboratory Standards (NCCLS). Nutrient agar plates were prepared, and the surfaces were evenly spread with a bacterial inoculum containing 10^6 CFU/ml of four selected *S. aureus* isolates using

a sterile swab. Wells 8 mm in diameter were created in the agar, and each well was filled with 100 µl of the ethanolic extract at a concentration of 25 mg/ml. After a 2-h diffusion period at room temperature, the plates were incubated at 37°C for 24 h. Inhibition zones, indicating bacterial growth inhibition, were measured in millimeters around the wells. Three replicates were performed for each organism to ensure reliable results.

Identification of MRSA isolates by the VITEK 2 compact automated antibacterial susceptibility test

The antibacterial susceptibility test was conducted using the VITEK 2 Compact system. Isolate suspensions were prepared and added to the antimicrobial susceptibility test card GP-67. The system automatically processed the samples and determined susceptibility to antibacterial drugs. The GP-67 card allowed for cefoxitin screening and oxacillin minimum inhibitory concentration (MIC) testing. The results were interpreted as sensitive or resistant based on Clinical and Laboratory Standards Institute recommendations. *S. aureus* ATCC29213 served as the quality control strain (Wayne. 2016).

Identification of by matrix-assisted laser desorption/ionization-time of flight (MALDI-TOF) mass spectrometry (MS) biotyper

The selected *S. aureus* isolate st.8 was identified via (MALDI-TOF–MS, database version 3, BioMerieux, France). The acquired spectra were analyzed on a VITEK MS IVD system. Single colonies were placed on a 48-well VITEK MS-DS disposable target slide and covered with VITEK MS alpha-cyano-4-hydroxycinnamic acid matrix. Confidence percentages between 90 and 98% were used for genus-level identification and > 98% for species-level identification, and < 90% of the results were considered unacceptable. For identifying the isolate, the peaks from the spectrum were compared to the standard spectrum for a certain species, genus, or family of microbe.

Animal model

Thirty-six healthy male albino rats, weighing between 130 and 170 g and aged 4 weeks, were obtained from the Al-Zyade Experimental Animals Production Center in Giza, Egypt. The rats were housed in clean polypropylene cages under controlled environmental conditions, including a temperature of 23 ± 2°C, a relative humidity of 55 ± 5%, and a 12:12-h light/dark cycle. The participants had unrestricted access to water and a standard diet. Prior to the experiment, the rats were acclimatized for 10 days. The Animal Care and Use Committee, Faculty of Veterinary Medicine, University of Sadat City, approved the experimental protocol, with the approval number VUSC-012-1-22.

Experimental design

An inoculum of the selected MRSA *Staphylococcus aureus* (st.8) was prepared by culturing the cells in nutrient broth at 37°C for 24 h. The harvested cells were counted to determine the viable inoculusm by plating suitable dilutions on nutrient agar and incubating them at 37°C for 24 h. The rats were divided into six groups, each containing six rats. Group A served as the control group and received normal saline orally for 14 days. Group B received *A. annua* NPs orally at a dose of 50 mg/kg for 14 days (Ranjbar et al. 2014). Group C received *A. annua* extract orally at a dose of 50 mg/kg for 14 days (Alshehri.2022). Group D was infected with *S. aureus* (MRSA st.8) by subcutaneous injection for 2 days (Hamouda et al. 2020). Group E was infected with *S. aureus* (MRSA st.8) for 2 days and then orally administered the *A. annua* ethanolic extract at a dose of 50 mg/kg for 15 days. Group F was infected with *S. aureus* (MRSA st.8) for 2 days and treated orally with *A. annua* AgNPs at a dose of 50 mg/kg for 14 days.

Blood sampling

At the end of the experiment, the rats were anesthetized, and blood samples were obtained from the inner eye can thus using heparinized capillary tubes. The collected blood was divided into two parts. The first part was left to clot at room temperature without anticoagulant. After clotting, the samples were centrifuged, and the clear serum was collected and stored at − 80°C for biochemical analysis. The second group of blood samples was drawn into EDTA tubes for hematological examination.

Hematological investigation

The hematological parameters evaluated in this study included the red blood cell (RBC) count, hemoglobin concentration (Hb), packed cell volume (PCV), and total and differential leukocyte counts. These parameters were assessed using a Sysmex XN hematology analyzer, which is a high-performing automated system. The XN-Series analyzer, manufactured by Sysmex in Kobe, Japan, incorporates the DI-60 automated digital cell imaging analyzer. This advanced technology enables automated processing of samples, complete blood counts (CBCs), slide preparation and staining, and digital scanning with pre-classification of cells.

Tissue samples

After the animals were euthanized, lung specimens were collected and rinsed with saline solution. The lung tissue was then divided into two parts for different analyses. One part was stored at − 80°C for assessing lipid peroxidation (MDA) and the activity of antioxidant enzymes (CAT and SOD) as markers of oxidative stress. The

second group of lung samples was preserved in 10% neutral buffered formalin for subsequent histopathological and immune histochemical examinations.

Determination lipid peroxidation (MDA) and the antioxidant defense system (CAT and SOD)

Kits were purchased from Biodiagnostic Company (Dokki, Giza, Egypt) to determine the MDA concentration (CAT. NoMD 25 29), CAT (CAT. No CA 25 17), SOD (CAT.No. SD 25 21).

Determination of tissue malondialdehyde (MDA)

Lipid peroxidation products such as malondialdehyde (MDA) were detected in lung homogenates according to the procedure described by Kei (1978), OhKawa et al. (1979) using biodiagnostic kits.

Determination of catalase activity

Catalase activity was determined in tissue homogenates (lungs) according to the procedure described by Aebi (1984) using biodiagnostic kits.

Determination of superoxide dismutase activity

Superoxide dismutase (SOD) content was determined in lung homogenates according to the procedure described by Nishikimi et al. (1972) using biodiagnostic kits.

Histopathological examination

At the end of the experiment, lung tissue samples were obtained from the different groups. The samples were fixed in 10% neutral buffered formalin and subjected to a series of processing steps, including washing, dehydration, clearing, and embedding in paraffin. The paraffin-embedded blocks were then sliced into 5-micron-thick sections. Histopathological examination was performed by staining the sections with hematoxylin and eosin following the protocol of Bancroft and Gamble (2008). The stained sections were observed and analyzed under a light microscope (Olympus BX50, Japan).

Histopathological lesion scoring

Histopathological changes in the lungs were assessed and categorized based on a scoring system: no changes (0), mild changes (1), moderate changes (2), and severe changes (3). The severity of changes was determined by the percentage of affected tissue: < 30% (mild change), < 30%–50% (moderate change), and > 50% (severe change) (Saleh et al. 2022).

Immunohistochemistry

The lung tissue sections were deparaffinized and rehydrated using alcohol. Antigen retrieval was performed by treating the sections with citrate buffer (pH 6) for 20 min. The sections were then incubated with the following specific antibodies: rabbit monoclonal anti-TNF-α (ab270264, dilution rate 1:100; Abcam, Cambridge, UK) and rabbit polyclonal anti-iNOS (ab15323, dilution rate 1:100; Abcam, Cambridge, UK) for two hours in a humidified chamber. Subsequently, the sections were incubated with goat anti-rabbit IgG H&L (HRP) (ab205718; Abcam, Cambridge, UK), and 3,3'-diaminobenzidine tetrahydrochloride (DAB) was used as a chromogen. The slides were counterstained with hematoxylin and mounted with DPX. Negative control slides were prepared by replacing the primary antibodies with PBS.

Evaluation of TNF-α and iNOS immunostaining

The levels of TNF-α and iNOS immune reactivity in tissue sections from each group were quantitatively assessed following the methods of Alshafei et al. (2023). A total of five tissue sections were analyzed. In each section, immunoreactivity was examined in 10 microscopic fields under high-power magnification (×400). The percentage of cells showing positive staining was determined using the color deconvolution feature of ImageJ 1.52p software developed by Wayne Rasband at the National Institutes of Health (U.S.A.).

Statistical analysis

The results were statistically analyzed by using one-way analysis of variance (ANOVA) followed by Duncan's post hoc test to confirm the significant differences among groups by using SPSS software (SPSS Version 16 released in 2007). A difference of $p < 0.05$ was considered to indicate statistical significance according to Snedecor and Cochran (1967). All the data are presented as the mean ± standard error (SE).

Results

Screening of *Staphylococcus aureus* isolates

Table 1 displays that 19 isolates (4, 9, 10, 13, 14, 15, 16, 17, 18, 19, 20, 21, 23, 24, 25, 26, 28, 29, and 30) were gram-negative bacilli, short rods, and nonspore-forming bacteria and tested for catalase based on their morphological examination. On the other hand, 11 isolates (numbers 1, 2, 3, 5, 6, 7, 8, 11, 12, 22, and 27) were gram-positive cocci found in clusters and showed a positive reaction to the catalase test, indicating a possible affiliation with the Staphylococci family. Among these, nine isolates (numbers 1, 2, 3, 6, 7, 8, 12, 22, and 27) exhibited beta hemolysis on blood agar media (Fig. 1a). Additionally, four isolates (8, 12, 22, and 27) were confirmed to ferment mannitol, as indicated by the change in the indicator phenol red to yellow, as shown in Fig. 1b. These isolates also tested positive according to the coagulase test. Moreover, the four selected isolates (numbers 8, 12, 22, and 27)

Table 1 Screening of *Staphylococcus aureus* isolates by biochemical tests

Bacterial isolate code	Gram staining	Catalase test	Blood hemolysis	MSA agar	Dnase test	Coagulase test
St.1	+ve	+ve	+ve	−ve	−ve	−ve
St.2	+ve	+ve	+ve	−ve	−ve	−ve
St.3	+ve	+ve	+ve	−ve	−ve	−ve
St.4	−ve	−ve	−ve	−ve	−ve	−ve
St.5	+ve	+ve	−ve	−ve	+ve	−ve
St.6	+ve	+ve	+ve	−ve	−ve	−ve
St.7	+ve	+ve	+ve	−ve	−ve	−ve
St.8	+ve	+ve	+ve	+ve	+ve	+ve
St.9	−ve	−ve	−ve	−ve	−ve	−ve
St.10	−ve	−ve	−ve	−ve	−ve	−ve
St.11	+ve	+ve	−ve	−ve	−ve	−ve
St.12	+ve	+ve	+ve	+ve	+ve	ve+
St.13	−ve	−ve	−ve	−ve	−ve	−ve
St.14	−ve	+ve	−ve	−ve	−ve	−ve
St.15	−ve	−ve	−ve	−ve	−ve	−ve
St.16	−ve	−ve	−ve	−ve	−ve	−ve
St.17	−ve	−ve	−ve	−ve	−ve	−ve
St.18	−ve	−ve	−ve	−ve	−ve	−ve
St.19	−ve	−ve	−ve	−ve	−ve	−ve
St.20	−ve	−ve	−ve	−ve	−ve	−ve
St.21	−ve	−ve	−ve	−ve	−ve	−ve
St.22	+ve	+ve	+ve	+ve	+ve	+ve
St.23	−ve	−ve	−ve	−ve	−ve	−ve
St.24	−ve	−ve	−ve	−−ve	−ve	−ve
St.25	−ve	−ve	−ve	−ve	−ve	−ve
St.26	−ve	−ve	−ve	−ve	−ve	−ve
St.27	+ve	+ve	+ve	+ve	+ve	+ve
St.28	−ve	−ve	−ve	−ve	−ve	−ve
St.29	−ve	−ve	−ve	−ve	−ve	−ve
St.30	−ve	−ve	−ve	−ve	−ve	−ve

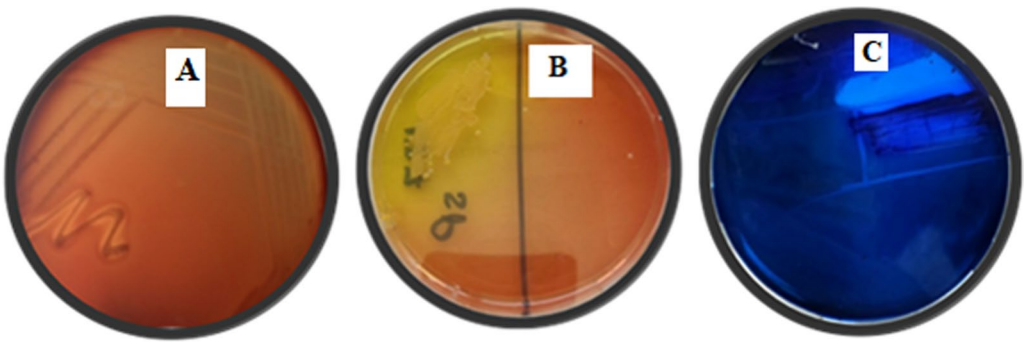

Fig. 1 Biochemical tests of selected local *Staphylococcus aureus* isolates on **A** Hemolysis on blood agar, **B** Mannitol salt agar test and **C** DNase test

were positive according to the DNase test, which was confirmed by the appearance of a clear zone around the growth area, indicating DNase activity (Fig. 1c). These four local isolates (numbers 8, 12, 22, and 27) were chosen for further experimentation in this study.

Phytochemical component of *Artemisia annua ethanolic* extract

The spectrum of identified major effective compounds of the *A. annua* ethanolic extract using a GC1300 mass spectrometer revealed nine major compounds, Table 2 and Fig. 2. These included 4,4-dimethyladamantan-2-ol produced at a retention time (RT) of 27.28 (with an area percentage of 5.13%), β-copaene observed at RT. of 2.68%. Otherwise, *n*-hexadecanoic acid found at RT. of 30.72 (with 12.74%), deoxyartemisinin noticed at RT. of 31.35 (with 3.75%). While 3,4-hexadienal, 2-butyl-2-ethyl-5-methyl was at RT of 32.18 (with 4.88%). Furthermore, 9-octadecenoic acid, methyl ester, (E) determined at R.T. of 32.52 (with 2.31%), oleic acid found at R.T. 33.80 (with 23.28%), octadecanoic acid found at R.T. 34.38 (with 7.30%), and finally 2,3-dihydroxypropyl elaidate recognized at R.T. 38.04 (with 1.93%).

Table 2 The spectrum of identified major effective compounds of *Artemisia annua* ethanolic extract using trace GC 1300-TSQ mass

No	*RT/min	Compound name	Area%	**MW	***MF
1	27.28	4,4-Dimethyladamantan-2-ol	5.13	180	$C_{12}H_{20}O$
2	29.88	β-copaene	2.68	204	$C_{15}H_{24}$
3	30.72	*n*-Hexadecanoic acid	12.74	256	$C_{16}H_{32}O_2$
4	31.35	Deoxyartemisinin (Qinghaosu C)	3.75	266	$C_{15}H_{22}O_4$
5	32.18	3,4-Hexadienal, 2-butyl-2-ethyl-5-methyl-	4.88	194	$C_{13}H_{22}O$
6	32.52	9-Octadecenoic acid, methyl ester, (E)-	2.31	296	$C_{19}H_{36}O_2$
7	33.80	Oleic Acid	23.28	282	$C_{18}H_{34}O_2$
8	34.38	Octadecanoic acid	7.30	324	$C_{21}H_{40}O_2$
9	38.04	2,3-Dihydroxypropyl elaidate	1.93	356	$C_{21}H_{40}O_4$

* Rt Retention time, ** MW molecular weight, *** MF molecular formula

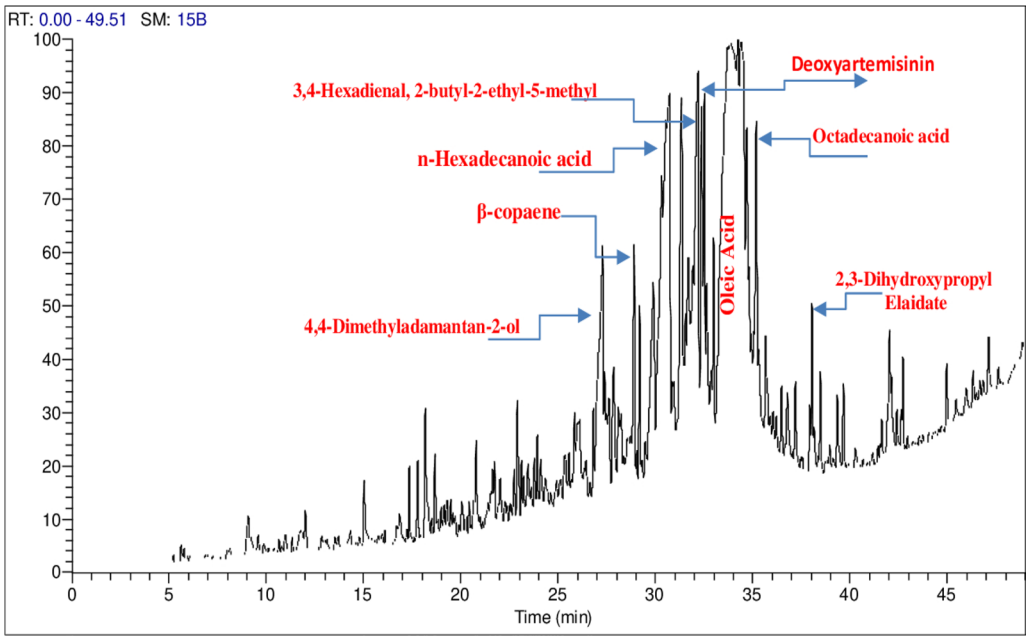

Fig. 2 The spectrum of identified compounds *Artemisia annua* ethanolic extract using trace GC 1300-TSQ mass

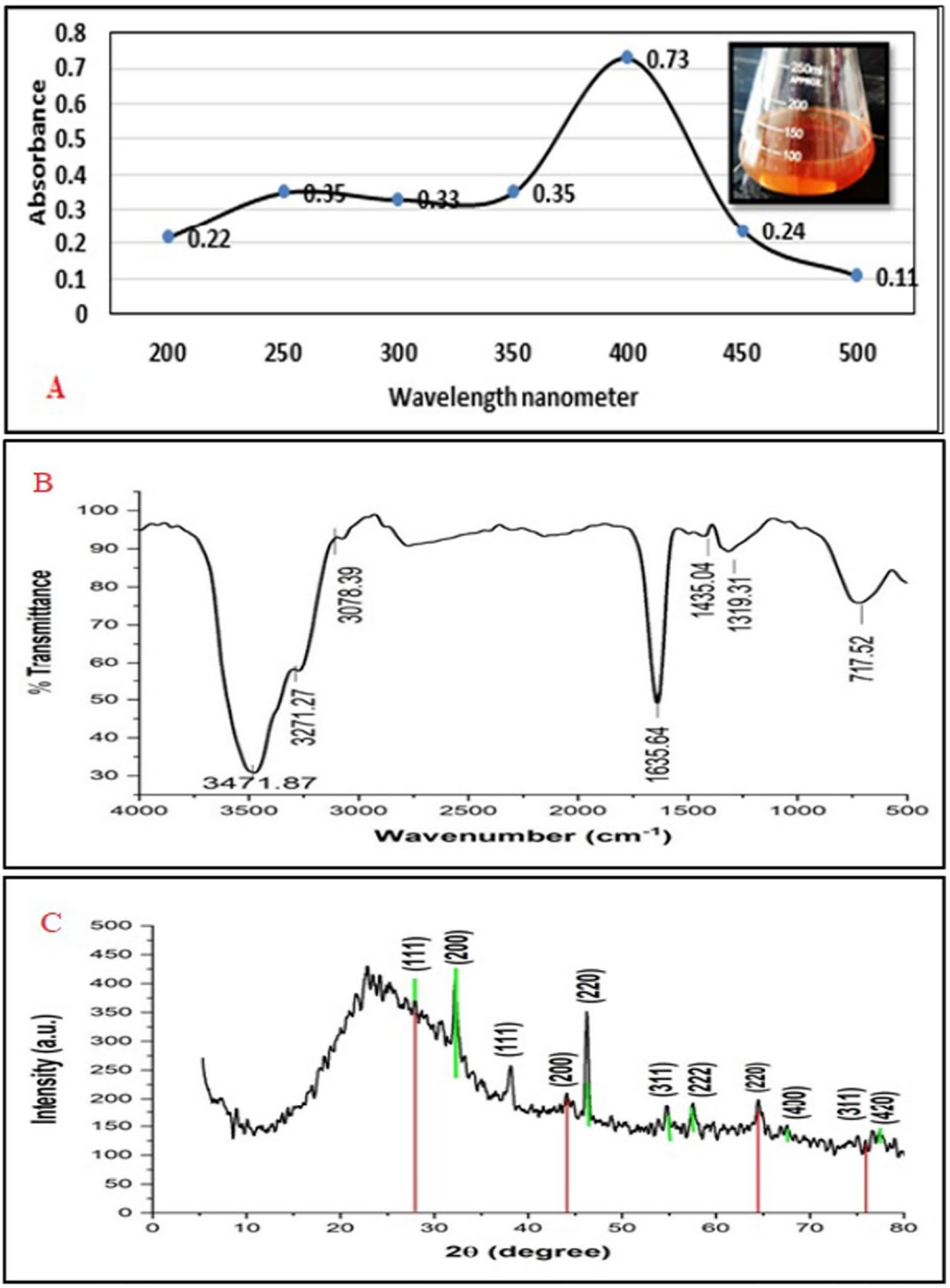

Fig. 3 **A** Green biosynthesis of AgNPs-based *A. annua* extract and UV–Vis absorption spectrum, **B** Fourier transform infrared spectroscopic peaks of AgNPs synthesized by *A.annua* extract. **C** XRD analysis of green AgNPs based on *A. annua* extract

Biofabrication and characterizations of silver nanoparticles based on the *Artemisia annua* extract

UV–Vis spectroscopy

The results in Fig. 3a demonstrate the formation of AgNPs, as indicated by a change in color to reddish brown upon utilizing the *A. annua* extract as a reducing agent. The maximum absorbance at 440 nm, which is characteristic of plasmon excitation of silver nanoparticles, was observed.

Fourier transform infrared (FTIR) spectroscopy

As shown in Fig. 3b, the spectra of the adsorbents were analyzed within the wavenumber range of 500–4000 cm^{-1}. The absorption peaks observed in the FTIR spectrum of the biologically synthesized AgNPs are presented. Notably, a significant upshift of the peak at 3434.78 cm^{-1} to a sharp peak at 3471.87 cm^{-1} was observed. The peak at 3078.39 cm^{-1} was attributed to the C-H stretching vibrations of aromatic compounds, while the sharp peak at 1635.64 cm^{-1} indicated the presence of the amide C=O carbonyl stretch group. Additionally, the absorption peak at 1319.31 cm^{-1} was characteristic of nitro compounds and their NO_2 stretching vibrations. Finally, the peak at 717.52 cm^{-1} was associated with the bending vibrations of aromatic CH bonds. Overall, the FTIR analysis revealed distinct absorption peaks during the biogenic synthesis of AgNPs.

X-ray diffraction of AgNPs

The crystalline properties of the green (AgNPs) were determined using X-ray diffraction (XRD), as illustrated in Fig. 3c. The XRD pattern displayed distinct Bragg reflections with 2θ values corresponding to the following peaks: 27.82, 32.24, 44.24, 54.83, 57.48, 67.46, 74.45, and 76.75. These peaks were attributed to the crystallographic planes of AgCl and Ag (111), Ag (200), AgCl (220), AgCl (222), AgCl and Ag (311), AgCl (400), AgCl and Ag (331), and AgCl and Ag (420). Notably, no chlorine-containing reagent was added during the synthesis of the AgNPs. Therefore, the presence of AgCl detected by XRD can be attributed to the reaction between the active substances present in the Artemisia extract and $AgNO_3$.

TEM examination

As shown in Fig. 4a, the synthesized AgNPs obtained using the *A. annua* extract exhibited a spherical shape with a diameter ranging (9 to 50 nm). TEM selected area electron diffraction (SAED) image confirmed the crystallinity of the silver nanoparticles as shown in Fig. 4b. Furthermore, the HR-TEM examination represented that synthesis of different range according to their polydisperse. The particle size distribution (PSD) was calculated that shows the percentage distribution and frequency of synthesized green nanoparticle sizes (1–50 nm) (Fig. 4c). SEM examination confirmed the presence of synthesized nanoparticles (Fig. 4d). The image shows agglomerates of small grains and dispersed nanoparticles, validating the findings from the TEM analysis in this study. The results in Fig. 4e show the elemental analysis of the AgNPs using EDX and reveal the composition of the Artemisia-based AgNPs. The analysis indicated the presence of 14.85% Ag, 26.71% oxygen, 19.46% carbon, 10.75% potassium, and 7.34% calcium. A prominent peak at 20 keV, which is typical of metallic silver nanoparticles, was observed. EDX analysis also detected additional optical absorption peaks corresponding to oxygen (O) and carbon (C) in the biomass after the adsorption of Ag ions.

Evaluation of the antibacterial activity of the new green Artemisia annua/ AgNPs in vitro

Results in Fig. 5a clarified that the ethanolic extract of *A. annua* (96%) had a significant and greater effect than the ethanolic extract (70%) on the four selected isolates and the indicator bacteria *E. coli* and *S. aureus* ATCC 25923. Additionally, the new nanoparticles exhibited better inhibitory activity against the St.8 isolate (18 mm) than against the other isolates. The St.12, St.22, and St.27 isolates showed significant lower antibacterial activity than the other treatments (with diameters ranging from 7 to 15 mm). The presence of AgNPs revealed the presence of a plant extract shell capping agent. As shown in Fig. 5b. Furthermore, the particles had a spherical shape with polydisperse and formed aggregates; adsorbed on the cell wall of st.8 isolate and coved the cell envelope, leading to leakage of the cellular content and loss their viability as in Fig. 5c. It was found that an *A.anuua* /AgNPs showed a maximum zone of inhibition against *S. aureus* (18 mm), followed by a ethanolic extract (96%) (17 mm) as gram-positive bacteria, whereas minimum activity was found in a AgNPs only (16 mm) against *S. aureus*.

Identification of MRSA St.8 by the VITEK2 compact automated system and MALDI–TOF MS

The results presented in Table 3 represented the identification of MRSA isolate st.8 using the VITEK2 compact automated system. The isolate exhibited resistance to three antibiotics and sensitivity to fifteen antibiotics. Specifically, it was resistant to cefotixin, oxacillin, and benzylpenicillin, indicating resistance to all β-lactams and cephalosporins according to CLSI (MRSA) guidelines. Conversely, St.8 showed sensitivity to fifteen antibiotics, as determined by the VITEK2 test. The results of MALDI-TOF MS the spectrum of the new MRSA *S. aureus* st 8 showed highly match through the reference spectra with confidence value up to 99.9% (Additional file 1).

Hematological effects of the ethanolic extract of Artemisia annua and A. annua /AgNPs in S. aureus-infected rats

Table 4 shows that, compared with those in the control group, the Hb concentration, RBC, hematocrit, and lymphocyte count ($p<0.05$) in the group infected with *S. aureus* were significantly lower. However, treatment of infected rats with *A. annua* and *A. annua*/AgNPs resulted in normalization of the hemoglobin (Hb)

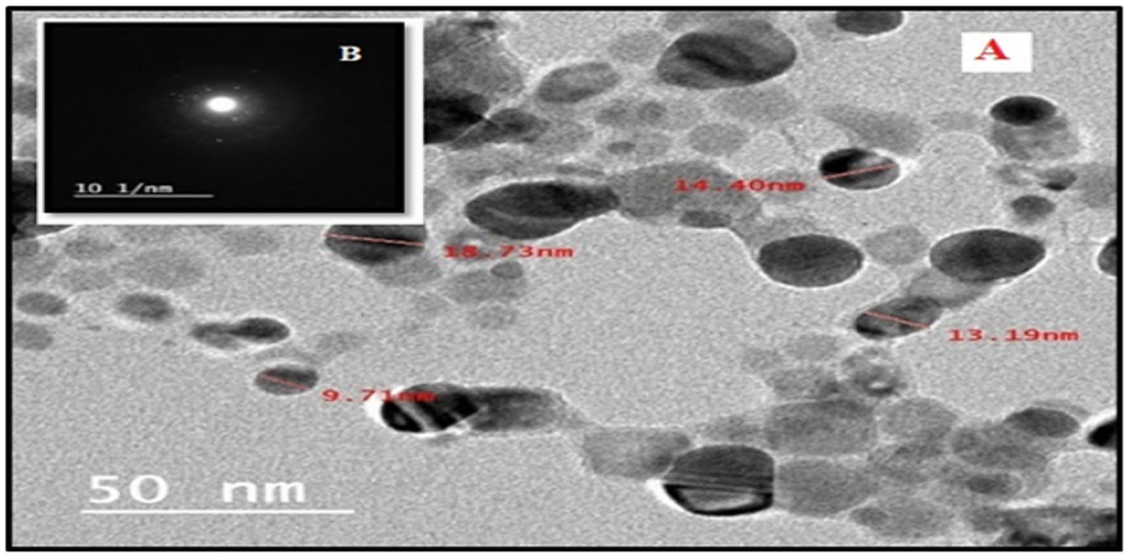

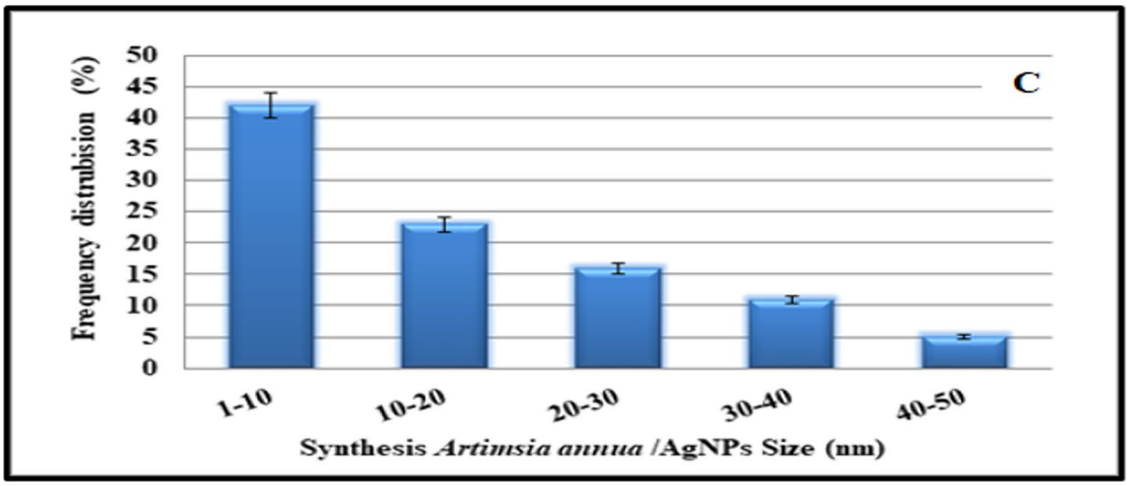

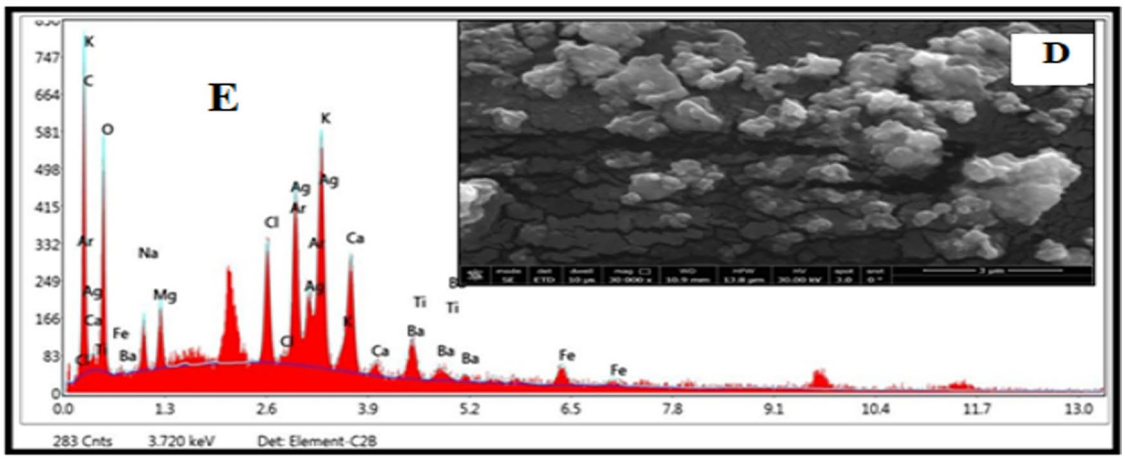

Elements	C	O	Na	Mg	Cl	Ag	K	Ca	Ba	Fe
Weight (%)	19.46	26.71	3.71	2.75	4.16	14.85	10.75	7.34	6.63	2.64

Fig. 4 **A** Green AgNPs based on *Artemisia annua* extract of AgNPs at 50 nm scale bar **B** TEM selected area electron diffraction image. **C** Frequency % and dispersion particles size **D** Scanning electron microscopy examination of AgNPs based on *A. annua* extract at 3 µm scale bar. **E** Elemental mapping of EDX analysis green AgNPs based on *A. annua* extract

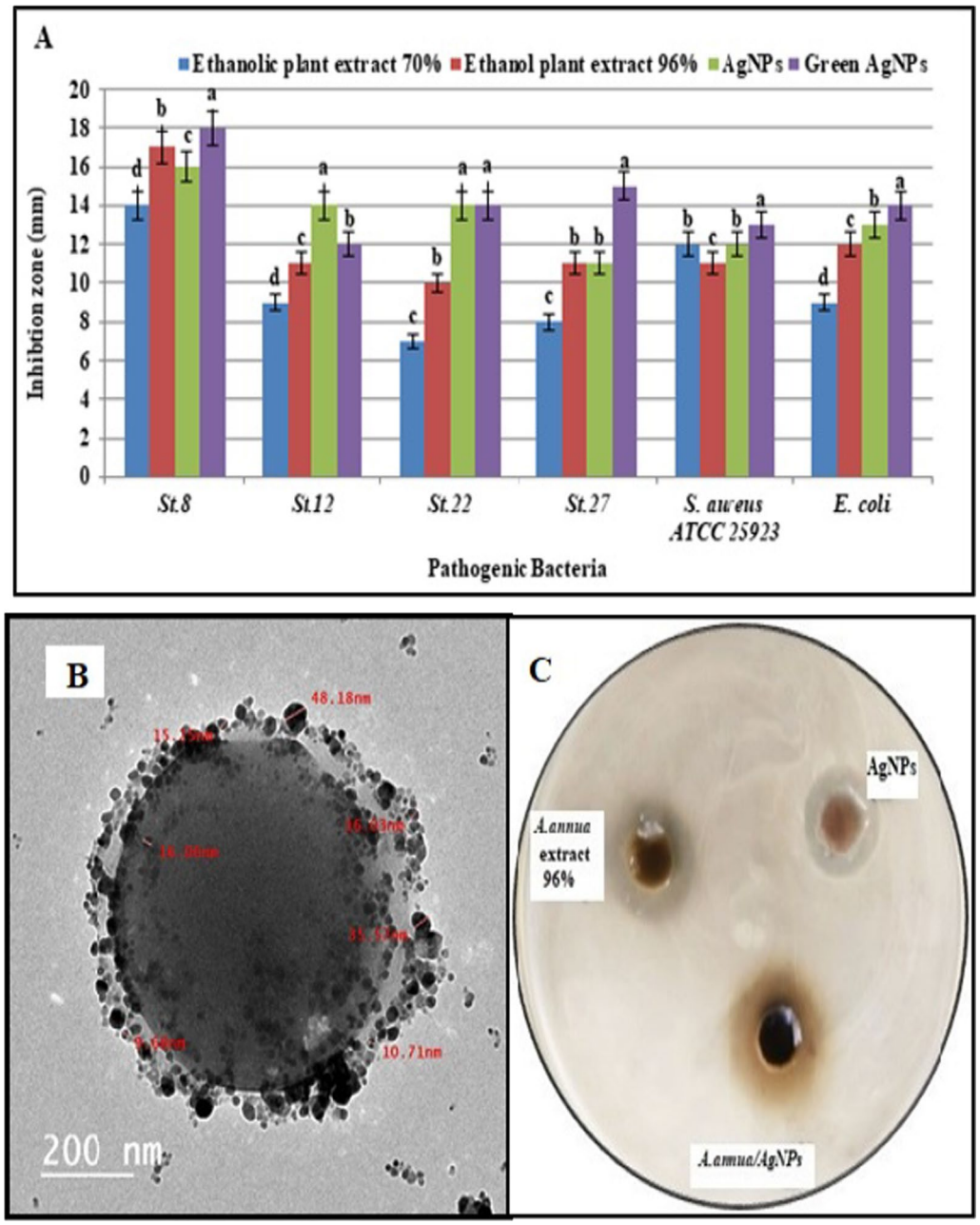

Fig. 5 **A** Antibacterial activity of green AgNPs based on *Artemisia annua* extract of AgNPs against selected isolates (8, 12, 22, 27) of *Staphylococcus aureus* and indicators bacteria (mm). The vertical bars represent standard errors of the means ($n = 3$). Bars followed by the same letter (s) are not significantly different ($p \leq 0.05$). **B** HR-TEM examination of new MRSA (st 8) isolate treated with AgNPs based on *A. annua* extract at 200 nm scale bar. **C** Bacterial growth inhibition zone achieved in agar well diffusion

concentration, red blood cell (RBC) count, hematocrit percentage, and lymphocyte count compared to those in the MRSA-infected group. Conversely, the results showed a significant increase in total leukocyte count, neutrophil count, and platelet count in the *S. aureus* infection group compared to those in the control group. However, supplementation of infected rats with *A. annua* and *A. annua* /AgNPs reduced the total leukocyte count, neutrophil count, and platelet count compared to those in the MRSA-infected group.

Table 3 Identification of selected MRSA isolate St .8 by VITEK2 compact automated system

Antibiotics	MIC (µg/ml)	Interpretation	Antibiotics	MIC (µg/ml)	Interpretation
Cefoxitin	0.5	Resistance	Erythromycin	0.25 ≥	Sensetive
Benzylpenicillin	0.5 ≤	Resistance	Clindamycin	0.25 ≥	Sensetive
Oxacillin	0.5	Resistance	Quinupristin/Dalfopristin	0.25 ≥	Sensetive
Gentamicin	0.5 ≥	Sensetive	Linezolid	2	Sensetive
Ciprofloxacin	0.5 ≥	Sensetive	Vancomycin	0.5 ≥	Sensetive
Levofloxacin	0.12 ≥	Sensetive	Tetracycline	1 ≥	Sensetive
Moxifloxacin	0.25 ≥	Sensetive	Tigecycline	0.12 ≥	Sensetive
Inducible Clindamycin resistance	0.11	Sensetive	Nitrofurantoin	16 ≥	Sensetive
Trimethoprim/sulfamethoxazole	10 ≥	Sensetive	Rifampicin	0.5 ≥	Sensetive

Table 4 Effect of ethanolic extract of *Artemisia annua and A. annua* silver nanoparticles and/or *S. aureus* on hematological parameters in rats

Parameter	GA	GB	GC	GD	GE	GF
Hb (g/dL)	13.27 ± 0.24^{a}	13.2 ± 0.26^{a}	13.63 ± 0.35^{a}	11.98 ± 0.18^{b}	13.8 ± 0.18^{a}	13.64 ± 0.30^{a}
RBCs ($\times 10^{6}/mm^{3}$)	6.76 ± 0.18^{ab}	6.46 ± 0.14^{bc}	7.37 ± 0.27^{a}	5.82 ± 0.21^{c}	6.9 ± 0.18^{ab}	6.9 ± 0.30^{ab}
HCT (%)	39.77 ± 0.49^{a}	39.62 ± 0.49^{a}	40.5 ± 0.29^{a}	36.97 ± 0.58^{b}	40.7 ± 0.23^{a}	40.43 ± 0.64^{a}
MCV (Fl)	58.8 ± 1.0^{bc}	60.23 ± 0.71^{ac}	55.04 ± 1.6^{b}	63.6 ± 1.4^{a}	$58.3 \pm 1.4b^{c}$	$58 \pm 1.6b^{c}$
MCH (pg)	19.62 ± 0.26^{ab}	20.16 ± 0.33^{b}	19.50 ± 0.24^{a}	20.62 ± 0.71^{b}	19.8 ± 0.31^{b}	19.5 ± 0.42^{ab}
MCHC (%)	33.3 ± 0.22^{ab}	33.28 ± 0.27^{ab}	33.65 ± 0.62^{a}	32.43 ± 0.43^{b}	34 ± 0.26^{a}	33.72 ± 0.34^{a}
WBCs($\times 10^{3}/mm^{3}$)	15.57 ± 0.78^{d}	14.4 ± 0.32^{de}	13.4 ± 0.32^{b}	32.5 ± 0.55^{a}	19.29 ± 0.43^{b}	17.3 ± 0.45^{e}
Lymphocyte ($\times 10^{3}/mm^{3}$)	84.83 ± 0.32^{a}	85.87 ± 0.18^{a}	86.1 ± 0.38^{a}	67.73 ± 0.89^{d}	81.57 ± 0.33^{c}	83.2 ± 0.1^{b}
Neutrophil ($\times 10^{3}/mm^{3}$)	15.16 ± 0.32^{d}	14.13 ± 13.4^{d}	13.9 ± 0.38^{d}	32.27 ± 0.9^{a}	18.4 ± 0.33^{b}	16.8 ± 0.1^{c}
Platelets ($\times 10^{3}$/mL)	653 ± 14.57^{c}	666 ± 5.78^{cd}	597 ± 7.8^{b}	740 ± 4.3^{a}	697 ± 2.9^{d}	614.3 ± 19.7^{b}

Values are expressed as means ± SE (standard errors). The mean difference is significant at $p < 0.05$. Data with different letters in the same row are significantly different. GA: (control group), GB: (*A. annua* nano silver group), GC: (*A. annua* extract group), GD: (MRSA-infected group), GE: (MRSA and *A. annua* extract group),GF: MRSA-infected and *A. annua* nanosilver new group). red blood cells (RBCs), hemoglobin concentration (Hb), packed cell volume (PCV), mean corpuscle volume (MCV), mean corpuscle hemoglobin (MCH), Mean corpuscle hemoglobin concentration (MCHC), white blood cells (WBCs)

Table 5 Effect of ethanolic extract of *Artemisia annua* and *A. annua* silver nanoparticles and/or *S. aureus* on oxidant/ antioxidant biomarkers in rats

Parameter	GA	GB	GC	GD	GE	GF
CAT	4.32 ± 0.13^{b}	4.70 ± 0.11^{ab}	4.90 ± 0.06^{a}	1.2 ± 0.12^{d}	2.66 ± 0.16^{e}	3.61 ± 0.21^{f}
SOD	72.67 ± 0.88^{a}	70 ± 0.58^{a}	69.3 ± 3.5^{a}	15.67 ± 0.88^{d}	28 ± 1.73^{c}	52.67 ± 5.54^{b}
MDA	0.66 ± 0.05^{d}	0.53 ± 0.06^{d}	0.61 ± 0.06^{d}	6.47 ± 0.46^{a}	3.87 ± 0.15^{b}	2.13 ± 0.34^{c}

Values are expressed as means ± SE (standard errors). The mean difference is significant at $p < 0.05$. Data with different letters in the same row are significantly different. GA: (control group), GB: (*A. annua* nano silver group), GC: (*Artemesia annua* extract group), GD: (MRSA infection group), GE: (MRSA and *A. annua extract* group),GF: MRSA and *A. annua* nano silver new group).Catalase(CAT),superoxide dismutase (SOD),malondialdehyde (MDA)

Assessment of the effects of ethanolic extracts of Artemisia annua and A. annua /AgNPs and/ or Staphylococcus aureus on oxidant/antioxidant biomarkers in rats

Table 5 shows that MRSA infection resulted in a significant increase in malondialdehyde (MDA) levels compared to those in the control group. However, the administration of *A. annua* and *A. annua* /AgNPs to infected rats led to a significant decrease in MDA levels compared to those in the infected group. Moreover, *S. aureus* infection caused a significant decrease in catalase (CAT) and superoxide dismutase (SOD) activity compared to that in the control group. Conversely, the administration of *A. annua* and *A. annua* /AgNPs to infected rats resulted in significant increases in CAT and SOD activity compared to those in the infected group.

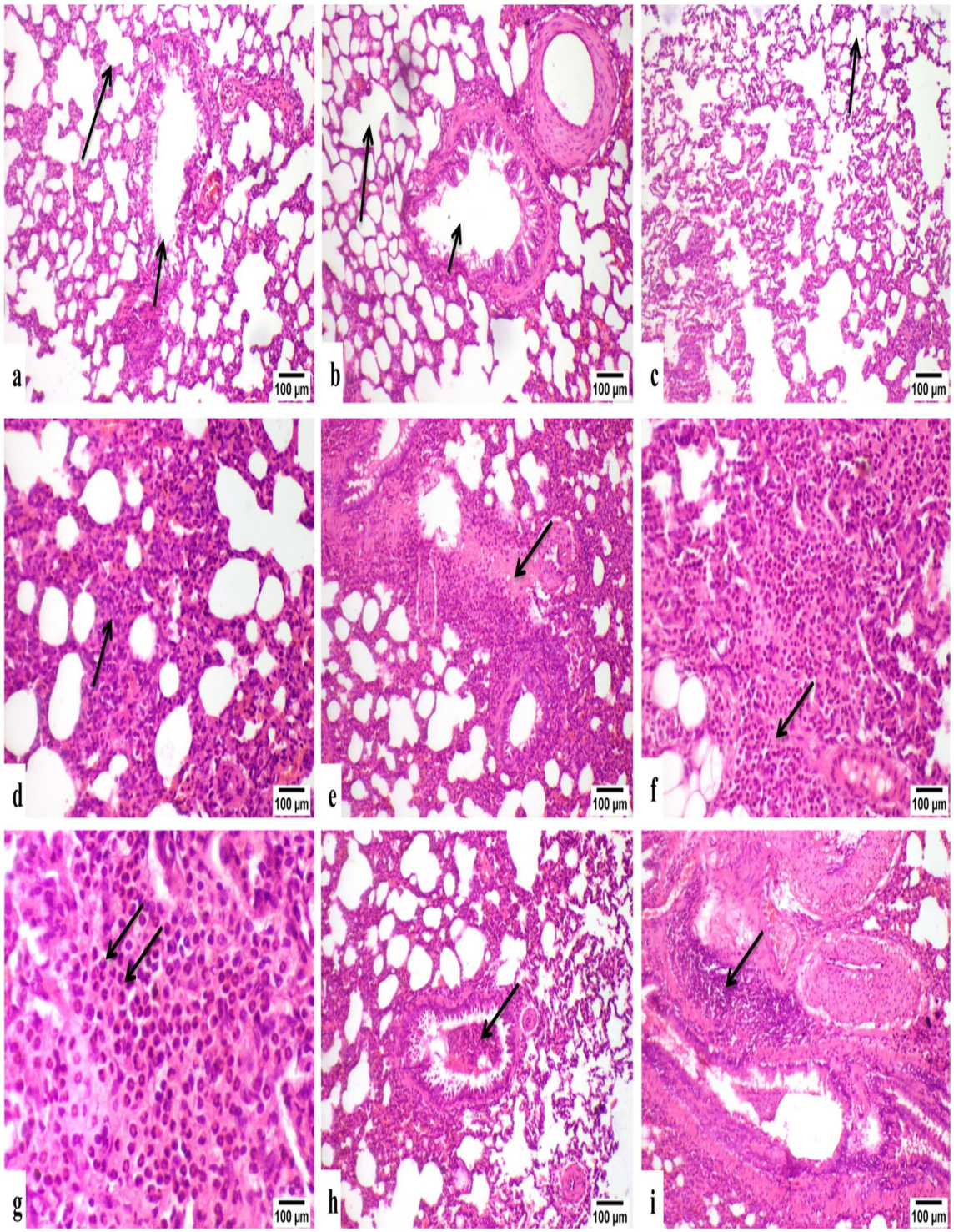

Fig. 6 Histopathological alterations scoring in lungs of treated groups photomicrograph, rat lungs **a, b** and **c** Groups A, B and C, respectively, showing normal histological structure of lung alveoli (long arrow) and bronchioles (short arrow) (H&EX100). **d** Group D showing thickening of interstitial tissue by inflammatory cells (arrow) (H&EX200). **e** Group D showing homogenous esinophilic area of liquifactive necrosis (arrow) (H&EX100). **f** higher magnification of the previous photo showing liquefaction and neutrophils infiltration (arrow) (H&EX200). **g** Group D showing presence of numerous inflammatory cells mainly polymorphonuclear inflammatory cells (arrows) (H&EX400). **h** Group D showing inflammatory exudate and inflammatory cells inside bronchiolar lumen (arrow) (H&EX100). **i** Group D showing peribronchiolar inflammatory cells infiltration (arrow) (H&EX200). (H&E scale bar 100 µm)

Histopathological findings

Histological assessment of lung tissues from the different experimental groups revealed that Groups A, B, and C had significant normal histological structures of lung alveoli and bronchioles, as shown in Fig. 6a–c, respectively. In contrast, Group D exhibited interstitial tissue thickening infiltrated by inflammatory cells (Fig. 6d). Additionally, homogeneous eosinophilic areas indicating liquefactive necrosis are presented in Fig. 6e, accompanied by infiltration of inflammatory cells, mainly neutrophils (Fig. 6f, g). Inflammatory exudate and inflammatory cells were observed inside the bronchiolar lumen (Fig. 6h), and peribronchiolar inflammatory cell infiltration was marked (Fig. 6i).

The bronchiolar lining epithelium showed hyperplasia and papillary folding, along with congestion of peribronchiolar blood vessels (Fig. 7a) Group E exhibited a small area of polymorphonuclear inflammatory cell aggregation (Fig. 7b), mild interstitial tissue thickening due to inflammatory cell infiltration (Fig. 7c), and minimal exudate in the bronchiolar lumen (Fig. 7d). Peribronchiolar inflammatory cell infiltration and mild bronchiolar epithelium hyperplasia were also observed (Fig. 7e). In Group F, notable significant improvements in the aforementioned lesions were observed, with nearly normal bronchiolar walls and empty bronchiolar lumens. Mild congestion of peribronchiolar blood vessels (Fig. 7f), minimal peribronchiolar inflammatory cell infiltration (Fig. 7g), and mild interstitial tissue thickening due to the presence of inflammatory cells (Fig. 7h) were obvious, indicating a recovery process. All recorded lesions in the lungs were scored according to their severity, as shown in Table 6.

Immunohistochemical findings of TNF-α and iNOS in the lungs

Immunostaining analysis of TNF-α and iNOS in the lungs revealed no immune reactive cells in Groups A, B, or C (Fig. 8a–c). In contrast, Group D exhibited strong expression of TNF-α and iNOS (Fig. 8d). Alternatively Groups E and F significant demonstrated moderate to weak positive immune reactions for TNF-α and iNOS in a few cells (Fig. 8e, f). The immunostaining for TNF-α and iNOS in the lung tissue of different experimental groups is depicted in Fig. 8g.

Discussion

MRSA is a significant pathogen that causes a range of illnesses in humans and animals. It initially manifests as a skin infection but can lead to serious conditions such as endocarditis, pneumonia, and septicemia (Shaaban et al. 2023). Plant-based synthesis of AgNPs offers advantages over chemical methods, including biological benefits, cost-effectiveness, and environmental friendliness (Allafchian et al. 2016). *Aannua* is effective at treating pulmonary damage and oxidative stress due to its antioxidant activities. It also has antimicrobial properties against various pathogens, including *Staphylococcus aureus*, making it a valuable traditional herbal medicine (Yang et al. 2015). Besides, the MALDI-TOF MS is a quick and extremely precise microbial identification technique for different soil, food and blood samples (Ahmed et al. 2021; Sabeq et al. 2022 ; Thelen et al. 2023).

The results of this investigation demonstrated that the *A. annua* ethanolic extract contains various bioactive compounds, such as flavonoids, amino acids, proteins, polyphenols, and vitamins, which act as reducing agents (Shaaban and El-Sharif. 2001). Silver nanoparticles and other composite nanoparticles of metals have been reported to possess antifungal, antibacterial, and antioxidant effects (Hassanen et al. 2020). The antibacterial activity of silver is attributed to its impact on the permeability of microorganism cell walls (Durán et al. 2016). Silver nanoparticles bind to thiol groups on cysteine residues, preventing bacterial DNA replication (Feng et al. 2000). Additionally, silver nanoparticles can induce oxidative stress and damage the respiratory chain, resulting in bactericidal effects (Moritz and Geszke 2013). Moreover, the combination of the *A. annua* extract with AgNPs exhibited significant antibacterial activity, which may be attributed to the interaction between the extract and other groups, such as the thiol group of the L-cysteine protein. This interaction could lead to enzymatic failure and cell death (Stevanović et al. 2012).

The successful synthesis of AgNPs using *A. annua* extract was confirmed through various characterization techniques, including SEM, TEM, XRD, UV–Vis, EDS, and FTIR, in this study. These techniques supported the observation of appropriate morphology, size, shape, and presence of elemental silver signals, while the *A. annua* extract acted as a capping agent. UV–Vis spectroscopy is a commonly used method for analyzing the structure of silver nanoparticles. The color change from yellow to brown in the silver nitrate and plant extract mixture was attributed to surface plasmon resonance, which is responsible for the color change (Vijayakumar et al. 2013). The absorption spectrum analysis revealed a prominent peak at 400 nm, indicating the presence of metal nanoparticles. This peak shifted to longer wavelengths as the particle size increased (Chung et al. 2016).

AgNPs with sizes ranging from 8–50 nm were successfully synthesized using plant extracts as reducing agents, resulting in a wide dispersion of spherical and quasi-spherical biogenic AgNPs, as reported previously (Lakshmanan et al. 2018). In addition, promising applications of nanoparticles have shown potential in cancer

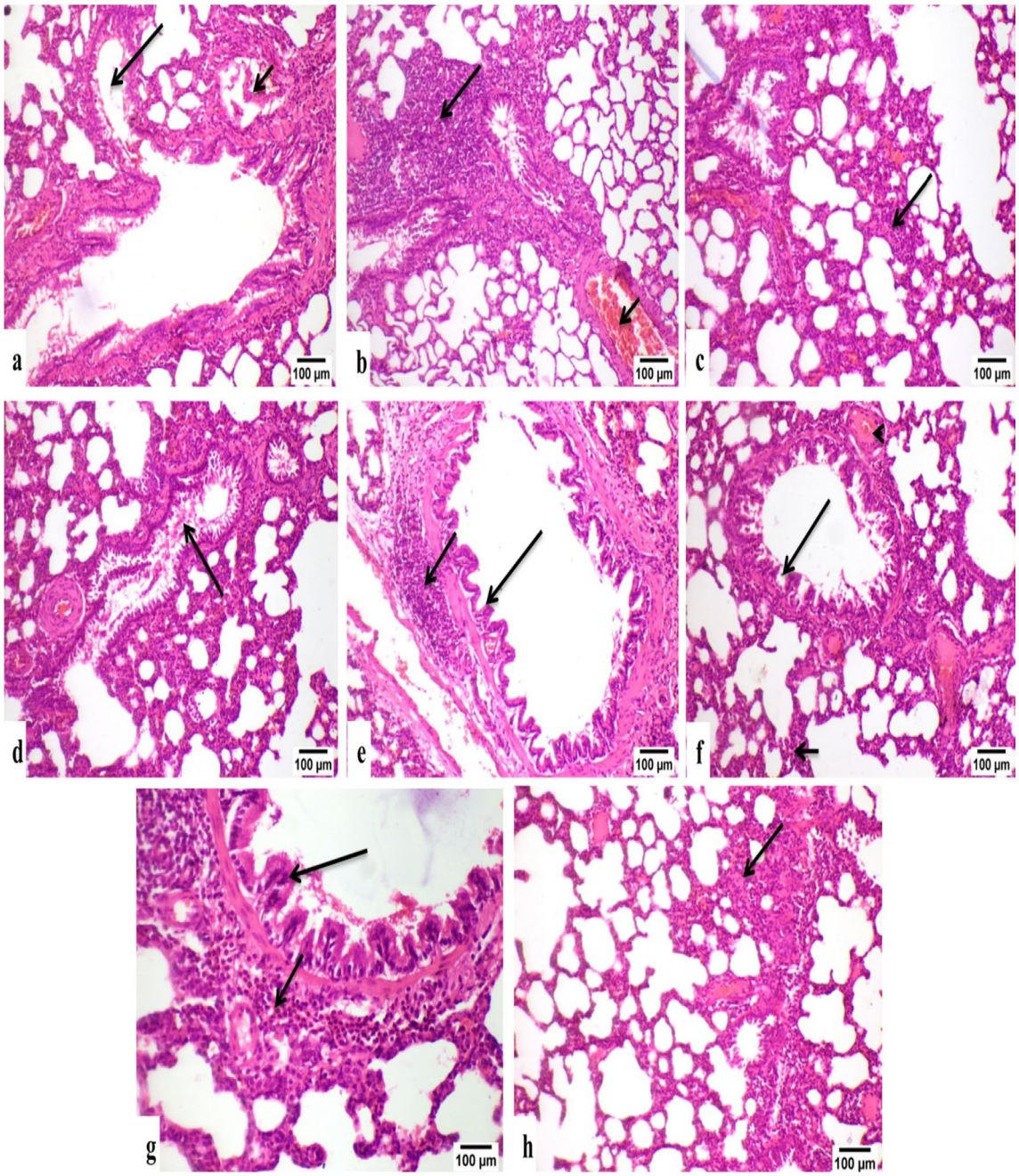

Fig. 7 Photomicrograph, rat lungs. **a** Group D showing bronchiolar epithelium hyperplasia (long arrow) and congestion of peribronchiolar blood vessels (short arrow). **b** Group E showing area of polymrphnuclear inflammatory cells aggregation (long arrow) with peribronchiiolar blood vessels congestion (short arrow). **c** Group E showing mild thickening of interstitial tissue by inflammatory cells (arrow). **d** Group E showing few exudate in bronchiolar lumen (arrow) **e** Group E showing few peribronchiolar inflammatory cells infiltration (short arrow) and mild bronchiolar hyperplasia (long arrow). **f** Group F showing normal bronchiolar wall with empty bronchiolar lumen (long arrow), mildly congested peribronchiolar blood vessels (arrowhead) and slightly thickened interstitial tissue (short arrow). **g** Group F showing slight bronchiolar wall hyperplasia (long arrow) and few peribronchiolar inflammatory cells infiltration (short arrow). **h** Group F showing mild thickening of interstitial tissue by inflammatory cells (arrow) (H&E scale bar 100 µm)

therapeutics as drug delivery systems. Various studies have shown that biogenic AgNPs synthesized from *A. annua* effectively suppress *S. aureus* and *E. coli* growth (Feng et al. 2000). Furthermore, these materials exhibited superior antibacterial activity compared to other biogenic AgNPs (Durán et al. 2016). In addition, AgNPs

Table 6 Histopathological alterations scoring in lungs of treated groups

Lesions	Treated rats groups					
	A	B	C	D	E	F
Thickening of interstitial tissue	0	0	0	3	1	1
Areas of liquefactive necrosis	0	0	0	2	1	0
Neutrophilic infiltration	0	0	0	3	2	1
Inflammatory exudate in bronchiolar lumen	0	0	0	2	1	0
Peribronchiolar inflammatory cells infiltration	0	0	0	2	1	1
Peribronchiolar vascular congestion	0	0	0	3	2	1
Bronchiolar wall hyperplasia	0	0	0	3	1	1

The score system was designed as: score 0 = absence of the lesion in all rats of the group ($n = 5$), score 1:(< 30%), score 2: (< 30%–50%), score 3: (> 50%)

were found to inhibit bacterial growth by causing DNA damage and disrupting cell membranes.

FTIR analysis revealed that the *A. annua* extract contains various functional groups, including aromatic compounds, amide bonds, carbonyl groups, and alkyl halides, which may act as reducing agents in the synthesis of silver nanoparticles, in agreement with the findings of Hamouda et al. (2020). These functional groups are involved in the creation and stability of AgNPs. GC–MS analysis confirmed the presence of antibacterial agents and antioxidants, such as glycyrrhetinic acid and ruspolinone, in the extract, which contributed to the enhanced antibacterial effect of the AgNPs.

It has been documented that *n*-hexadecanoic acid (palmitic acid) has various bioactive effects, including anti-inflammatory, antioxidant, hypocholesterolemic, nematicidal, pesticidal, antiandrogenic, flavoring, hemolytic, 5-alpha reductase inhibitory, potent antimicrobial, antimalarial, and antifungal effects (Abo-Dahab 2014). *A. annua*, a renowned medicinal plant, is valued for its production of artemisinin (Qinghaosu), a cadinane-type sesquiterpene lactone with an endoperoxide bridge. Artemisinin is notably effective against chloroquine- and quinine-resistant Plasmodium falciparum and other malaria-causing parasites (Willcox et al. 2004). Moreover, it has been reported that Oleic acid and 9-octadecenoic acid (E) serve as 5-alpha reductase inhibitors, possess allergenic properties, exhibit anti-inflammatory and antiandrogenic effects, and contribute to anemia prevention. These compounds also demonstrate anti-alopecic properties, inhibit leukotriene-D4, act as choleretics, cause dermatitis, are hypocholesterolemic, function as insect repellents, are used in perfumery, aid in treating alopecia, and serve as flavoring agents (Rahman et al. 2014).

EDX analysis demonstrated the presence of silver and other oxides, indicating the formation of metallic silver nanoparticles along with the organic constituents of the *A. annua* extract in this study, while XRD analysis confirmed the crystalline nature of the new AgNPs, with distinct diffraction peaks corresponding to the face-centered cubic structure of silver (Allafchian et al. 2016).

This study aimed to investigate the protective effect of *A. annua*-loaded silver nanoparticles against *S. aureus*-induced pulmonary damage. The infected group showed a decrease in RBC count; Hb, PCV, MCV, MCH, and MCHC values, indicating microcytic hypochromic anemia. This can be explained by hyperplasia of the mononuclear phagocytic system, which leads to increased iron storage and reduced iron transfer to erythroid cells (El-Naser and Khamis 2009). An increase in the total leucocyte count is primarily due to neutrophilia, eosinophilia, and monocytosis, which are associated with bacterial infections and acute inflammatory disorders (Raghib et al. 2004). The stress-induced release of corticosteroids and histamine release from microbial hypersensitivity may contribute to leukocytosis and eosinophilia (Alshehri 2022). The lymphocyte count reduction observed in the present study is consistent with previous findings, indicating the redistribution of lymphocytes to lymphoid tissues and contributing to lymphopenia (Sayed et al. 2002). *S. aureus*, known for its ability to produce hemolysin, can target and kill host cells. The untreated infected groups showed decreased Hb, RBC, platelet, and PCV levels, which may be due to RBC lysis during infection or iron depletion inhibiting erythropoiesis during our investigation. *S. aureus* can utilize hemoglobin as a source of iron. An elevated ESR, TLC, and neutrophil count are reliable indicators of infection and normalize after effective treatment (Saleh et al. 2022).

Oxidative stress arises from an imbalance between ROS production and the antioxidant system. One study confirmed increased MDA levels and decreased SOD and CAT activity in the MRSA-infected group, indicating oxidative stress (Santos et al. 2009). AgNPs treatment reduced lipid peroxidation and restored SOD and CAT

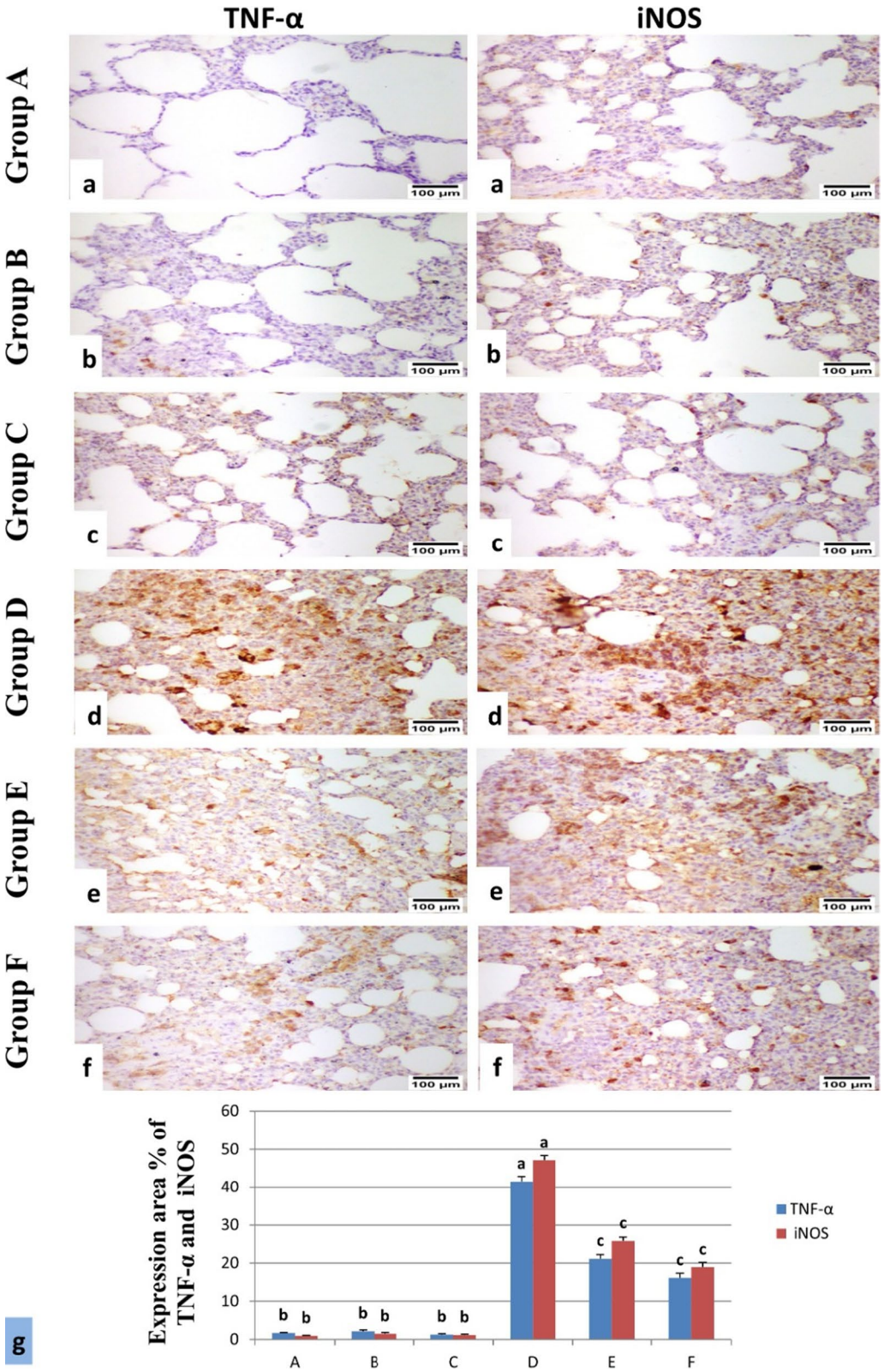

Fig. 8 Immunostaining of TNF-α and iNOS, rat lungs. **a, b** and **c** Groups A, B and C, respectively, showing very weak to nil immune reactive cells. **d** Group D showing strong expression of TNF-α and iNOS. **e** and **f** Groups E and F, respectively, showing moderate to weak positive immune reaction in few cells (TNF-α and iNOS scale bar 100 µm). **g** Immunostaining expression area % of TNF-α and iNOS (data were expressed as mean ± SE, different letters (a, b, c) indicating significant differences at $p < 0.05$. (H&E scale bar 100 µm)

activity, suggesting that these compounds have antioxidant effects. The decrease in SOD activity may be due to free radical removal, while CAT effectively converts H_2O_2 to oxygen and water. The decrease in antioxidant enzyme activity could be attributed to substrate depletion, transcriptional downregulation, enzyme inactivation by MRSA-induced NO production, or a combination of factors (Ashakumari et al. 1996).

Histopathological examination of the lungs of the *S. aureus*-infected group revealed thickening of the interstitial tissue, liquifactive necrosis areas infiltrated by inflammatory cells, the presence of neutrophils, inflammatory exudate, and inflammation in the bronchiolar lumen. These findings align with previous studies by Hassanen and Ragab (2021), who reported *S. aureus* as a cause of bacteraemia and pneumonia, often leading to abscess formation. Neutrophils play a crucial role in the host's defense against *S. aureus* infection (Han et al. 2009), and the inflammatory response commonly manifests as abscess formation and is characterized by the presence of neutrophils, bacterial colonies, necrotic cell debris, and inflammatory exudates (Vinay et al. 2005).

Furthermore, Artemisia-loaded nanoparticles reversed the pulmonary effects caused by *S. aureus*. This effect may be attributed to their antioxidant activity, as evidenced by the reduction in MDA concentration and increase in SOD and catalase activities. These findings are consistent with those of Kim et al. (2014), who reported similar antioxidant effects. The antioxidant effect of Artemisia can be attributed to the presence of phenolic compounds such as coumarin, camphor, retinal O, 2-hydroxy-1,3-propanediyl ester/2,3-dihydroxypropyl elaidate/oleic acid, 3-hydroxypropyl ester/hexadecanoic acid, 2-hydroxy-1-(hydroxymethyl)ethyl ester/oleic acid, 3-hydroxypropyl ester/2 h-1-benzopyran-2-one, 7-hydroxy-6-methoxy, and isopropyl linoleate (Bisht et al.2021). These compounds have antioxidant and anti-inflammatory properties. Hexadecanoic acid methyl ester, a fatty acid ester found in Artemisia, has been shown to inhibit the growth of pathogenic bacteria. Furthermore, 2,6-diethenyl-1,4-benzenediol and 2,3-dimethylhydroquinone are alkyl *p*-hydroquinones that act as chain-breaking antioxidants and electron donors for redox intermediates, contributing to the antioxidant activity of Artemisia. Furthermore, Artemisia species also contain flavonoid compounds, which are known for their antioxidant properties. Previous studies have highlighted the presence of phenolics and flavonoids in Artemisia, which contribute to its antioxidant activity and have beneficial effects on reducing inflammation (Carvalho et al.2011).

In addition to its antioxidant activity, Artemisia also exhibits anti-inflammatory effects. This can be attributed to its ability to inhibit proinflammatory markers such as TNF-α and iNOS. Immunohistochemical findings in this study revealed strong expression of TNF-α and iNOS, which are considered proinflammatory markers (Madkour et al. 2022; Azouz et al. 2023).

Conclusions

In conclusion, the results demonstrated successful isolation and identification of a new MARS strain from the local Egyptian community using VITEK2 and Maldi-tof assay of the isolate st.8 as *Staphylococcus aureus*. Green AgNPs were successfully synthesized from *A. annua* extract, and their antibacterial and antioxidant activities were evaluated. The *A. annua* /AgNPs were characterized using UV–Vis spectroscopy, HR-FTIR, XRD, TEM, SEM, and EDX. The results showed that the AgNPs were spherical in shape with a diameter ranging from 9 to 48 nm. The *A. annua* / AgNPs also showed significant antibacterial activity against the new MRSA strain, which was better than that of the control or chemical AgNPs treatment. Additionally, the *A. annua* /AgNPs exhibited antioxidant properties, which may be beneficial for addressing the complications associated with *S. aureus*-induced pneumonia. The results confirmed that *A. annua* /AgNPs significantly normalized hematological parameters, increased antioxidant biomarkers, reduced interstitial tissue thickening via inflammatory cells. But *A. annua* /AgNPs had a weak positive immune reaction in a few cells (TNF-α and iNOS in rats compared to those in the infected group). GC-mass analysis confirmed by, where *A. annua* extract was shown to contain a variety of compounds, that have anti-inflammatory and antioxidant activities. Overall, the study suggested that green AgNPs generated from *A. annua* extract might be a promising therapeutic option for combating MRSA infections and reducing the reliance on antibiotics.

Abbreviations

Abcam	A biotechnology company
AgNPs	Silver nanoparticles
A. Annua	*Artemisia annua*
Artemisia annua/AgNPs	*A. annua*/AgNPs
ATCC	American Type Culture Collection
CAT	Catalase activity
CFU/ml	Colony-forming units per milliliter
DAB	3,3′-Diaminobenzidine tetrahydrochloride
EDTA	Ethylenediaminetetraacetic acid
EDX	Energy-dispersive X-ray spectroscopy
EUCAST	European Committee on Antimicrobial Susceptibility Testing
FTIR	Fourier transform infrared spectroscopy
GC–MS	Gas chromatography-mass spectrometry
GP-67	Antimicrobial susceptibility test card used in VITEK 2
Hb	Hemoglobin
HRP	Horseradish peroxidase
HR-TEM	High-resolution transmission electron microscopy
ICU	Intensive care unit
IgG	Immunoglobulin G

iNOS	Inducible nitric oxide synthase
MALDI-TOF MS	Matrix-assisted laser desorption/ionization-time of flight mass spectrometry
MDA	Malondialdehyde
MIC	Minimum inhibitory concentration
MRSA	Methicillin-resistant *Staphylococcus aureus*
NCCLS	National Committee for Clinical Laboratory Standards
PBS	Phosphate-buffered saline
PCV	Packed cell volume
RBCs	Red blood cell count
SOD	Superoxide dismutase
SPSS	Statistical Package for the Social Sciences
TNF-α	Tumor necrosis factor alpha
UV-Vis Spectrometer	Ultraviolet-visible spectrometer
VITEK 2	A brand of automated antibacterial susceptibility testing system
XRD	X-ray diffraction

Supplementary Information

The online version contains supplementary material available at https://doi.org/10.1186/s40543-024-00436-2.

Additional file 1. Identification of new isolate MRSA Staphylococcus aureus (st 8) by (MALDI-TOF-Ms Biotyper®) mass spectrum compared with reference spectra.

Acknowledgements
The authors extend their sincere appreciation to the Department of Microbial Biotechnology, Genetic Engineering, and Biotechnology Research Institute at the University of Sadat City, the Department of Biochemistry and Nutrition at the Faculty of Veterinary Medicine, University of Sadat City. Menoufyia University's Department of Botany and Microbiology deserves our sincere appreciation for their expert guidance and invaluable assistance throughout the research endeavor.

Author contributions
MTS contributed to conceptualization, experimental design, and data interpretation. MSA contributed to conceptualization, experimental design for microbial identification, nanoparticles synthesis, and characterizations. SHO contributed to conceptualization, experimental design for the animal model, and statistical analyses. RMK contributed to conceptualization, experimental design for histopathology. RHE conducted experimental work and contributed to data collection and manuscript writing. All authors critically reviewed and revised the manuscript.

Funding
Open access funding provided by The Science, Technology & Innovation Funding Authority (STDF) in cooperation with The Egyptian Knowledge Bank (EKB). Open access funding provided by The Science, Technology & Innovation Funding Authority (STDF) in cooperation with The Egyptian Knowledge Bank (EKB).

Data availability
The datasets used and/or analyzed during the current study are available from the corresponding author on reasonable request.

Declarations

Ethics approval and consent to participate
Committee (IACUC) with oversight of the faculty of Veterinary Medicine, University of Sadat City. Ethical approval number: (VUSC-012-1-22).

Competing interests
The authors have no relevant financial or non-financial interests to disclose.

Received: 7 November 2023 Accepted: 1 April 2024
Published online: 25 April 2024

References

Abd El-Kareem MS, Rabbih MAEF, Selim ETM, Elsherbiny EAEM, El-Khateeb AY. Application of GC/EIMS in combination with semi-empirical calculations for identification and investigation of some volatile components in basil essential oil. Int J Anal Mass Spectrom Chromatogr. 2016;4(1):14–25. https://doi.org/10.4236/ijamsc.2016.41002.

Abo-Dahab NF. GC–MS analysis of bioactive compounds of Aspergillus terreus var. Aureus isolated from Artemisia annua L. Afr J Mycol Biotech. 2014;19(3):17–29.

Adoni M, Yadam M, Gaddam SA, Rayalacheruvu U, Kotakadi VS. Antimicrobial, antioxidant, and dye degradation properties of biosynthesized silver nanoparticles from *Artemisia annua* L. Lett Appl NanoBioSci. 2020;10:1981–92. https://doi.org/10.33263/LIANBS101.19811992.

Aebi H. Catalase in vitro. Methods Enzymol. 1984;105:121–6. https://doi.org/10.1016/S0076-6879(84)05016-3.

Ahmed SO, Nasser AA, Abbas RN, Kamal MM, Zahran MA, Sorour NM. Production of bioconcrete with improved durability properties using Alkaliphilic Egyptian bacteria. 3 Biotech. 2021;11:231–45. https://doi.org/10.1007/s13205-021-02781-0.

Allafchian A, Mirahmadi-Zare S, Jalali S, Hashemi S. Green synthesis of AgNPs using *Phlomis* leaf extract and investigation of their antibacterial activity. J Nanostruct Chem. 2016;6:129–35. https://doi.org/10.1007/s40097-016-0187-0.

Alshafei MM, Mabrouk AM, Hanafi EM, Ramadan MM, Korany RM, Kassem SS, Mohammed DM. Prophylactic supplementation of microencapsulated *Boswellia serrata* and probiotic bacteria in metabolic syndrome rats. Food Biosci. 2023;51: 102325. https://doi.org/10.1016/j.fbio.2022.102325.

Alshehri MA. Cardioprotective properties of *Artemisia herba* alba nanoparticles against heart attack in rats: a study of the antioxidant and hypolipidemic activities. Arch Microbiol. 2022;29(4):2336–47. https://doi.org/10.1016/j.sjbs.2021.12.009.

Appalasamy S, Lo KY, Cheng SJ. Antimicrobial activity of artemisinin and precursor derived from in vitro plantlets of *Artemisia annua* L. Biomed Res Int. 2014. https://doi.org/10.1155/2014/215872.

Arciola CR, Campoccia D, Montanaro L. Implant infections: adhesion, biofilm formation and immune evasion. Arch Microbiol. 2018;16(7):397–409. https://doi.org/10.1038/s41579-018-0019.

Aromal SA, Philip D. Green synthesis of gold nanoparticles using Trigonella foenum-graecum and its size-dependent catalytic activity. Spectrochim Acta A Mol Biomol Spectrosc. 2012;97:1–5.

Ashakumari LS, Rao BS, Rao BS. Antioxidant enzyme response to gastric ulcers in rats: role of S-allyl cysteine. Arch Microbiol. 1996;210(6):859–68.

Ashraf JM, Ansari MA, Khan HM, Alzohairy MA, Choi I. Green synthesis of silver nanoparticles and characterization of their inhibitory effects on AGEs formation using biophysical techniques. Sci Rep. 2016;6:20414. https://doi.org/10.1038/srep20414.

Asif A, Asghar M, Khan HU. Antibiotic susceptibility pattern of clinical isolates of methicillin-resistant *Staphylococcus aureus* in Peshawar, Pakistan. Ann Roman Soc Cell Biol. 2021;25(6):20116–31.

Azouz RA, Korany RMS, Noshy PA. Silica Nanoparticle-induced reproductive toxicity in male albino rats via testicular apoptosis and oxidative stress. Arch Microbiol. 2023;201(4):1816–24. https://doi.org/10.1007/s12011-022-03280-w.

Baede VO, David MZ, Andrasevic AT, Blanc DS, Borg M, Brennan G, Enger H. MRSA surveillance programmes worldwide: Moving towards a harmonised international approach. Arch Microbiol. 2022;59: 106538. https://doi.org/10.1016/j.ijantimicag.2022.106538.

Bahrulolum H, Nooraei S, Javanshir N, Tarrahimofrad H, Mirbagheri VS, Easton AJ, Ahmadian G. Green synthesis of metal nanoparticles using microorganisms and their application in the agrifood sector. J Nanobiotechnol. 2021;19(1):1–26.

Bancroft JD, Gamble M. Theory and practice of histological techniques. 6th ed. Elsevier: Churchill Livingstone; 2008.

Baptista PV, McCusker MP, Carvalho A, Ferreira DA, Mohan NM, Martins M, Fernandes AR. Nano-strategies to fight multidrug-resistant bacteria "a

battle of the titans." Arch Microbiol. 2018;9:1441. https://doi.org/10.3389/fmicb.2018.01441.
Bisht D, Kumar D, Kumar D, Dua K, Chellappan DK. Phytochemistry and pharmacological activity of the genus Artemisia. Arch Pharmacal Res. 2021;44(5):439–74.
Carvalho IS, Cavaco T, Brodelius M. Phenolic composition and antioxidant capacity of six *Artemisia* species. Ind Crops Prod. 2011;33:382–8. https://doi.org/10.1016/J.Indcrop.2010.11.005.
Castillo-Henríquez L, Alfaro-Aguilar K, Ugalde-Álvarez J, Vega-Fernández L, Montes deOca-Vásquez, G, Vega-Baudrit JR. Green synthesis of gold and silver nanoparticles from plant extracts and their possible applications as antimicrobial agents in the agricultural area. Nanomaterials 2020;10(9):1763.
Chung IM, Park I, Seung-Hyun K, Thiruvengadam M. Plant-mediated synthesis of AgNPs: characteristic properties and therapeutic applications. Nanoscale Res Lett. 2016;11:40. https://doi.org/10.1186/s11671-016-1257-473-4.
Durán N, Durán M, De Jesus MB, Seabra AB, Fávaro WJ, Nakazato G. Silver nanoparticles: a new view on mechanistic aspects of antimicrobial activity. Nanomedicine. 2016;12(3):789–99. https://doi.org/10.1016/j.nano.2015.11.016.
El-Naser HH, Khamis AH. Hematological and biochemical changes in mice induced by single and combined infection of *Pasteurella multocida* and *Streptococcus pneumoniae*. Arch Microbiol. 2009;191(4):85–92. https://doi.org/10.1007/s00203-009-0459-7.
Feng QL, Wu J, Chen GQ, Cui FZ, Kim TN, Kim JO. A mechanistic study of the antibacterial effect of silver ions on *Escherichia coli* and *Staphylococcus aureus*. J Biomed Mater Res. 2000;52:662–8. https://doi.org/10.1002/1097-4636(20001215)52:4%3C662::aid-jbm10%3E3.0.co;2-3.
Goswami S, Bhakuni RS, Chinniah A, Pal A, Kar SK, Das PK. Anti-helicobacter pylori potential of artemisinin and its derivatives. Antimicrob Agents Chemother. 2012;56(9):4594–607. https://doi.org/10.1128/aac.00407-12.
Hamouda RA, Yousuf WE, Mohammed AA, Mohammed RS, Darwish DB, Abdeen EE. Comparative study between zinc oxide nanoparticles synthesis by biogenic and wet chemical methods *in vivo* and *in vitro* against *Staphylococcus aureus*. Arch Microbiol. 2020;147: 104384. https://doi.org/10.1016/j.micpath.2020.104384.
Han G, Martinez LR, Mihu MR, Friedman AJ, Friedman JM, Nosanchuk JD. Nitric oxide releasing nanoparticles are therapeutic for Staphylococcus aureus abscesses in a murine model of infection. Arch Microbiol. 2009;194(11): e7804. https://doi.org/10.1371/journal.pone.0007804.
Hassanen EI, Ragab E. *In vivo* and *in vitro* assessments of the antibacterial potential of chitosan-silver nanocomposite against methicillin-resistant *Staphylococcus aureus*–induced infection in rats. Bio Trace Element Res. 2021;199(1):244–57.
Hassanen EI, Morsy EA, Hussien AM, Ibrahim MA, Farroh KY. The effect of different concentrations of gold nanoparticles on growth performance, toxicopathological and immunological parameters of broiler chickens. 2020. Arch Microbiol. https://doi.org/10.1042/BSR20194296.
Holt JG, Krieg NR, Senath PHA, Staley JT, Williams ST. Bergey's manual of determinative bacteriology, 9th Ed. MD: Williams and Wilkins Baltimore, USA;1994.
Kei S. Lipid peroxides in cerebrovascular disorders determined by a new colorimetric method. Clin Chim Acta. 1978;90:37–43. https://doi.org/10.1016/0009-8981(78)90081-5.
Kim MH, Seo JY, Liu KH, Kim JS. Protective effect of *Artemisia annua* L. extract against galactose-induced oxidative stress in mice. Arch Microbiol. 2014;199(7):e101486. https://doi.org/10.1371/journal.pone.0101486.
Kim S, Lee SY, Cho HJ. Doxorubicin-wrapped zinc oxide nanoclusters for the therapy of colorectal adenocarcinoma. Arch Microbiol. 2017;7(3):1–15. https://doi.org/10.3390/nano7110354.
Lakshmanan G, Sathiyaseelan A, Kalaichelvan PT, Murugesan K. Plant-mediated synthesis of silver nanoparticles using fruit extract of *Cleome viscosa* L.: assessment of their antibacterial and anticancer activity. Karbala Int J Mod Sci. 2018;4:61–8. https://doi.org/10.1016/j.kijoms.2017.10.007.
Liu WT, Chen EZ, Yang L, Peng C, Wang Q, Xu Z, Chen DQ. Emerging resistance mechanisms for 4 types of common anti-MRSA antibiotics in *Staphylococcus aureus*: A comprehensive review. Microb Pathog. 2021;156: 104915. https://doi.org/10.1016/j.micpath.2021.104915.
Loges LA, Silva DB, Paulino GVB, Landell MF, Macedo AJ. Polyketides from marine-derived *Aspergillus welwitschiae* inhibit *Staphylococcus aureus* virulence factors and potentiate vancomycin antibacterial activity *in vivo*. Microb Pathog. 2020;143: 104066. https://doi.org/10.1016/j.micpath.2020.104066.
Madkour DA, Ahmed MM, Orabi SH, Alkafafy M, Korany RMS, Khalifa HK. Emamectin benzoate-induced hepatotoxicity in rats with special reference to protective potential of *Nigella sativa* oil. Arch Microbiol. 2022;195(3):4607–18. https://doi.org/10.12681/jhvms.28100.
Moritz M, Geszke-Moritz M. The newest achievements in synthesis, immobilization, and practical applications of antibacterial nanoparticles. Chem Eng J. 2013;228:596–613. https://doi.org/10.1016/j.cej.2013.05.046.
Nishikimi M, Rao NA, Yagi K. The occurrence of superoxide anion in the reaction of reduced phenazine methosulfate and molecular oxygen. Biochem Biophys Res Commun. 1972;46(2):849–54. https://doi.org/10.1016/s0006-291x(72)80218-3.
Obeid S, Alen J, Nguyen VH, Pham VC, Meuleman P, Pannecouque C. Artemisinin analogues as potent inhibitors of in vitro hepatitis C virus replication. PLoS ONE. 2013;8(12): e81783. https://doi.org/10.1371/journal.pone.0081783.
Ohkawa H, Ohishi N, Yagi K. Assay for lipid peroxides in animal tissues by thiobarbituric acid reaction. Anal Biochem. 1979;95(2):351–8. https://doi.org/10.1016/0003-2697(79)90738-3.
Perez C, Pauli M, Bazerque P. An antibacterial assay by agar well diffusion method. Arch Microbiol. 1990;15:113–5.
Raghib MF, Said EA, Hassan MS, Al-Gharabawy BS. Effect of pasteurellosis on health performance and some hematological and blood serum constituents of dromedary camel. Arch Microbiol. 2004;178(5–6):385–95.
Rahman MM, Ahmad SH, Mohamed MTM, Ab Rahman MZ. Antimicrobial compounds from leaf extracts of *Jatropha curcas*, *Psidium guajava*, and *Andrographis paniculata*. Sci World J. 2014. https://doi.org/10.1155/2014/635240.
Ranjbar A, Ataie Z, Khajavi F, Ghasemi H. Effects of silver nanoparticle (Ag NP) on oxidative stress biomarkers in rat. Arch Microbiol. 2014;1(3):205–10. https://doi.org/10.7508/nmj.2014.03.011.
Recio MC, Rios JL, Villar A. Antimicrobial activity of selected plants employed in the Spanish Mediterranean area. Part II. Phytother Res. 1989;3(3):77–80. https://doi.org/10.1002/ptr.2650030302.
Rushdy AA, Salama MS, Othman AS. Detection of methicillin/oxacillin-resistant Staphylococcus aureus isolated from some clinical hospitals in Cairo using Meca/Nuc genes and antibiotic susceptibility profile. Int J Agric Biol. 2007;9(6):800. https://doi.org/10.1155/2017/2191532.
Sabeq I, Awad D, Hamad Ahme, Nabil M, Aboubakr M, Abaza M, Fouad M, Hussein A, Shama S, Ramadan H, Edris S. Prevalence and molecular characterization of foodborne and human-derived *Salmonella* strains for resistance to critically important antibiotics. Transbound Emerg Dis. 2022;69:2153–2163. https://doi.org/10.1111/tbed.14553
Saleh N, Allam T, Korany RMS, Abdelfattah AM, Omran AM, Abd Eldaim MA, Hassan AM, El-Borai NB. Protective and therapeutic efficacy of hesperidin versus cisplatin against Ehrlich ascites carcinoma-induced renal damage in mice. Pharma. 2022;15(3):294. https://doi.org/10.3390/ph15030294.
Santos CX, Anilkumar N, Zhang M, Brewer AC, Shah AM. Redox signaling in cardiac myocytes. Arch Microbiol. 2009;193(4):375–81. https://doi.org/10.1016/j.freeradbiomed.2011.01.003.
Sayed RH, Khalil MA, El-Gohary OA, Hussein AS, El-Anwar N. Redistribution of lymphocyte subpopulations in acute leukemia. Arch Microbiol. 2002;159(1):42–6. https://doi.org/10.1038/sj.thj.6200140.
Shaaban MT, El-Sharif ME. Antimicrobial potencies of leaf extracts of some medicinal plants in Egypt against microorganisms of alternative representation in their phyllospheres. Afr J Mycol Biotechnol. 2001;9(2):15–25.
Shaaban MT, Zayed M, Salama HS. Antibacterial potential of bacterial cellulose impregnated with green synthesized silver nanoparticles against S. aureus and P. aeruginosa. Curr Microbiol. 2023;80(2):75. https://doi.org/10.1007/s00284-023-03182-7.
Shelembe B, Mahlangeni N, Moodley R. Biosynthesis and bioactivities of metal nanoparticles mediated by *Helichrysum aureonitens*. J Anal Sci Technol. 2022;13:8. https://doi.org/10.1186/s40543-022-00316-7.
Snedecor GW, Cochran WG. Statistical methods. Ames: Iowa State University Press; 1967.
Srikar SK, Giri DD, Pal DB, Mishra PK, Upadhyay SN. Green synthesis of silver nanoparticles: a review. Green Sustain Chem. 2016;6:34–56. https://doi.org/10.4236/gsc.2016.61004.

Stevanović MM, Škapin SD, Bračko I, Milenković M, Petković J, Filipič M, Uskoković DP. Poly (lactide-co-glycolide)/silver nanoparticles: synthesis, characterization, antimicrobial activity, cytotoxicity assessment, and ROS-inducing potential. Polymer. 2012;53(14):2818–28. https://doi.org/10.1016/j.polymer.2012.04.057.

Tao A, Song Z, Feng X, Zhang A, He H, Chen Y. Antibacterial and antiviral activities of *Artemisia Annua* aqueous extract *in vitro*. IOP Conf Ser Earth Environ Sci. 2020;565(1): 012053. https://doi.org/10.1088/1755-1315/565/1/012053.

Thelen P, Graeber S, Schmidt E. Hamprecht A. A side-by-side comparison of the new VITEK MS PRIME and the MALDI Biotyper sirius in the clinical microbiology laboratory. Eur J Clin Microbiol Infect Dis. 2023;42;1355–1363. https://doi.org/10.1007/s10096-023-04666-x

Turner NA, Sharma-Kuinkel BK, Maskarinec SA, Eichenberger EM, Shah PP, Carugati M, Fowler VG Jr. Methicillin-resistant *Staphylococcus aureus*: an overview of basic and clinical research. Nat Rev Microbiol. 2019;17:203–18. https://doi.org/10.1038/s41579-018-0147-4.

Vijayakumar M, Priya K, Nancy F, Noorlidah A. Biosynthesis, characterization, and antibacterial effect of plant-mediated AgNPs using *Artemisia nilagirica*. Ind Crops Prot. 2013;41:235–40. https://doi.org/10.1016/j.indcrop.2012.04.017.

Vijayalakshmi R, Rajendran V. Synthesis and characterization of nano-TiO2 via different methods. Arch Microbiol. 2012;4(2):1183–90.

Vinay K, Abbas AK, Fauston N, Aster JC. Robbins and cotran pathologic basis of disease. India pp: New Delhi; 2005. p. 628–36.

Wayne PA. Clinical and Laboratory Standards Institute (CLSI), Performance Standards for Antimicrobial Susceptibility Testing, CLSI supplement M100S. Clinical and Laboratory Standards Institute, Wayne, PA;2016.

Willcox M, Bodeker G, Bourdy G, Dhingra V, Falquet J, Ferreira JF. Wright CW *Artemisia annua* as a traditional herbal antimalarial. Trad Med Plants Malaria. 2004;4:43–59.

Yang C, Hu DH, Feng Y. Antibacterial activity and mode of action of *Artemisia capillaris* essential oil and its constituents against respiratory tract infection-causing pathogens. Mole Med Rep. 2015;11(4):2852–60. https://doi.org/10.3892/mmr.2014.3103.

Zhang Z, Li H, Guo D. 4-Mercaptobenzoic acid-modified Au@Ag nanoparticle-based colorimetric Cr3+ ions detection in aqueous solution. J Anal Sci Technol. 2023;14:40. https://doi.org/10.1186/s40543-023-00386-1.

Publisher's Note